

# PROBABILISTIC MODELING OF DRIVER BEHAVIORS AT URBAN CROSSROAD INTERACTIONS

Yuan-Cheng Liu, Kuei-Yuan Chan<sup>1</sup>,  
Department of Mechanical Engineering,  
National Taiwan University, Taipei, Taiwan

The interactions with human drivers is one of the major challenges for autonomous vehicles. In this work we consider urban crossroads without signals where driver interactions are indispensable. Crossroads are parameterized to be used in studying how drivers passing the crossroad while maintaining a desired speed without collision. We define a probability of yielding for each car as a function of vehicle speed and the distance-to-intersection for both vehicles, while the interactions between vehicles are characterized by a point of action for incoming vehicles from different directions. Driver behaviors in terms of acceleration/deceleration given current circumstances are also modeled probabilistically. The method is then analyzed and validated by data collected from human drivers in the simulated environments. The result shows comparable prediction accuracy to the state-of-the-art method, where characteristic parameters of drivers are also shown to be critical for the behavior predictions. We also extend our model to two real world urban crossroads applications : crash analysis and traffic characteristic parameters identification. In both cases, our prediction results are analogous to those acquired in virtual environments. For autonomous vehicle, our method can help building a computer driving logic that matches human behaviors such that interactions between different drivers will be more intuitive.

**Keywords:** autonomous vehicle, mixed-fleet, probabilistic model, driver behavior, crossroad, interaction model, collision avoidance.

---

<sup>1</sup>Corresponding Author, chanky@ntu.edu.tw, Fax:+886-2-2363-1755

## Symbols

$A$	adjustment term for the TFA distribution
$a_i$	acceleration of the $i^{\text{th}}$ vehicle
$C1_{R_{\min}}$	safe margin coefficient
$C2_{R_{\min}}$	safe margin constant
$C1_{\text{adec}}$	deceleration coefficient
$C2_{\text{adec}}$	deceleration constant
$d_{\text{node},i}$	displacement of the $i^{\text{th}}$ vehicle
min TTC	minimum TTC
$\oplus$	the node, point of intersection
$P_{\text{yield}}$	probability of yielding
POY	probability of yielding
$\Phi_{\mu,\sigma^2}$	CDF of the TFA distribution
$R_{\text{CA}}$	classification accuracy rate
$R_i$	braking distance
$R_{\min}$	safe margin
$\mathbf{S}_i$	states of the $i^{\text{th}}$ vehicle
$\tau$	reaction time
TTC	time to collision
TFA	time for action
$\text{TFA}_{\text{est}}$	estimated mean value of the TFA distribution
$v_i$	velocity of the $i^{\text{th}}$ vehicle

# 1 Introduction

The development of autonomous vehicles has grown rapidly as enabling technology emerges [1]. Optimists claim that by 2030, most human drivers will be replaced by autonomous vehicles, while road congestion, accidents due to human errors, and air pollution problems can all be resolved[2]. To date, more than 47 autonomous vehicle companies are testing their self-driving cars in urban California [3] in 2019. However, practitioners believe that the penetration rate of fully-autonomous vehicles will remain low for the next decades. According to the work of Bansal et al. [4], fully autonomous vehicles might take longer than expected to be ready in the market. Long-term (year 2015-2045) adoption rate of connected and autonomous vehicles (CAVs) under different scenarios is predicted to be 24.8% at level 5 (as defined by the US Department of Transportation [5]) by 2045. Regardless of the timeline of autonomous vehicles to be of great effects, evaluating the impact of autonomous vehicles needs to be done at a higher level, namely, how do people perceive and move around with autonomous vehicles, vehicles driven by computers?

Impacts of autonomous vehicles have been assessed in various aspects of transportation. From the original intentions of reducing the number of accidents due to human errors, to alleviate traffic congestions[6, 7]. However, if we consider the adaptation of autonomous vehicles from a city point of view, the impact might not all that positive. Studies argued that the reduction in the cost of traveling is likely to increase the total traveling distances for passengers which in turn exacerbate the congestion problem in urban areas[8, 9].

In all scenarios, autonomous vehicles ultimately have to share the roads with human drivers. Apart from the fact that the technology itself is still at a preliminary stage where no commercially available level 4 vehicles exist in the market, neither are policy, infrastructure, and consumer acceptance ready for high adoption rate [10]. As a consequence, it is foreseeable that the *mixed traffic flow* with both computer and human drivers will comprise the major part of the traffic during the transition stage that lasts for more than 30 years. Therefore, interactions between autonomous vehicles and the human environment will be the major challenge.

All new participants need to blend in the current traffic setup smoothly. Urban traffic scenarios that include lane merging/diverging, roundabouts, and crossroads without signals, rely heavily on driver interactions to predict and react accordingly. For example in Fig.1 we see an unsignalized crossroad for which drivers perceive and predict the possible intentions of others (shown as arrows in the figure), and then decide whether to accelerate or brake. These hints, as perceived by human drivers, are not understandable to autonomous vehicles nowadays, which might post a threat to surrounding drivers.

The main reason for autonomous vehicles being potential threats to other road users is that they do not understand the meanings behind human behaviors and can not foresee their intentions. According to the report by the state of California Department of Motor Vehicles (DMV), 18 of the 33 filed accidents with autonomous vehicles in 2019 (as of June 17, 2019) are rear-ended[3]. Most accidents (over 60%) happened as autonomous vehicles yielded unnecessarily for situations that following human drivers apparently did not anticipate. Autonomous vehicles are designed to drive conservatively for the cause of safety, but when those behaviours are not understandable to human drivers, over conservative autonomous vehicles become a new threat.

To prevent the problem addressed, interactions with surrounding agents should be achieved by understanding their behaviors. Decisions based on purely control logics such



Figure 1: A crossroad with no signal.

as traditional collision avoidance systems suffer from insufficient reaction time as reported in [11]. To warn drivers early enough to take proper actions, behavior prediction models are used, for example see pedestrians predictions in [12, 13, 14]. In these studies, pedestrian crossing intentions are identified and modeled, making their behaviors comprehensible and thus greatly improve the safety of road users. Driver behaviors are also crucial for making safe decisions in traffic flow [15, 16].

Although modeling human intentions have been the focus of several existing studies, these models are however based on either extensive data collections that are difficult to adapt to new environments or implicit model framework that are intractable for on-line application. We study driver behaviors at unsignalized crossroads and build explicit probabilistic models in this work. Proper behavior model should enable computer drivers to understand and to interact with human drivers more smoothly, resulting in a safer human-computer mixed traffic flow. In what follows, we reviewed driver models in Section 2; our proposed probabilistic driver behavior models in unsignalized crossroads are presented in Section 3; Section 4 provides extensions of the driver model on some real world applications; Section 5 concludes the study with future work.

## 2 Motion Prediction Models

Motion planning for autonomous vehicles has been studied extensively to provide optimal and collision-free trajectories[17]. Most algorithms assume known trajectories of all surrounding agents, while in fact we have very limited information about vehicles around us. Predicting surrounding vehicles' movements enables more active and more practical traffic studies. In the following section, based on the method employed, motion prediction models are classified into three main categories, namely physics-based models, driver behavior models and interactive models.

### 2.1 Physics-Based Models

Physics-based motion predictions use dynamic or kinematic models governed by simple physics laws as surveyed by Lefèvre et al. in [18]. These physics-based models predict the possible motion of the surrounding agents adopt linear-velocity models for their efficiency, friendliness in use, and good accuracy in short-term predictions[19, 20]. However, they do not account for uncertainties in real traffic with other human drivers. Zhan et al. use probability models of yielding/passing actions at a crossroad[21]. Other prediction models such as the work of Ruf et al. [22] use a cost map with probabilistic values on each path to optimize the global planner of vehicle movements. Although physics-based models are easier and cheaper to be applied, they suffer from poor long-term predictions, therefore have little interactions between the ego vehicle and other agents.

### 2.2 Driver Behavior Models

Motion predictions with driver behavior models on gas pedals/braes/steers along a path are the intent recognition processes based on the previous and current states of the target agents. Possible behaviors of surrounding agents are listed with a likelihood measure such as Bayesian networks or hidden Markov Model (HMM). Such models can be used, as an example, to estimate the chance of a vehicle violating a stop sign with dynamic Bayesian network (DBN) without extensive trajectory predictions [23]. Dagli et al. [24] used the same concept in building vehicle following and lane changing models with sensor data uncertainty as well as uncertainties in human behaviors. Their study is assessed in simulated lane changing experiments where the driver behaviors is recognized 1.5 seconds earlier than the actual lane change. Gindele et al. [25] use DBN, combined with the manually formulated models and models learned with random forest tree, to estimate and predict the driver behaviors of two cars passing an intersection.

### 2.3 Interactive Models

Long-term predictions have been achieved using interactive models with other agents. For example, at a vehicle might decide to pass an intersection because he/she believes that other vehicles are very likely to brake. Probabilistic methods such as partially observable Markov decision process (POMDP) have been used as the core of interactive models to determine the actions of an ego vehicle by predicting the future states of other agents. Foka et al. use FOMDP to navigate in a space with obstacles in [26]. Hubmann et al. use POMDP to evaluate the possible maneuvers of other agents and optimize the actions of the ego vehicle in [27]. However, POMDP is computationally expensive and therefore unable to be used for real-time predictions. In addition, vehicle drivers need to predict

the trajectories of only nearby vehicles, instead of all, a downsized POMDP application with only nearby vehicles is needed.

## 2.4 Explicit Driver Behavior Models

Behavior models provide driver intent for predictions in urban intersection that form the basics for current advance driver assistance systems (ADAS). Liebner et al. use intelligent driver models (IDM) for probability of turning and car-following behaviors in a simple Bayes net in [28] with different intention probabilities in arbitrary intersections with general speed profiles. To overcome driver behavior change, the features of different agents, such as speed, distance to the intersection, are extracted by Graf et al. in the process of case-based reasoning (CBR) for site-specific intersections[29]. CBR relates a case with similar experiences to predict the behavior of the driver. However, the results learned from one intersection still may not directly applicable for other intersections. Drivers with different driving style also affect the prediction accuracy significantly.

## 2.5 Summary

Despite the explicit formulation and general applicability, physics-based models can not account for states changes of the subject, which results in the poor long-term prediction. Interactive models with joint behaviors of surrounding agents could achieve better long-term predictions, with the sacrifice of computational cost and unable to handle large state spaces. Driver behavior models, on the other hand, have better long-term estimations than physics-based models 2.1 and better computational efficiency than interactive models 2.3 trained models are, however, only applicable to environments where the training data are extracted. More general and explicit driver behavior models at various traffic scenarios are needed to smoothly blend into urban traffic with mixed fleet. Each driver needs to understand the behaviors and intentions of other road users so that they can and react accordingly.

Autonomous vehicles nowadays do have the ability to resolve some potential threats, actively maneuver vehicles to avoid obstacles; however, they usually do so with no regard of what the maneuvers are perceived by human drivers. While technology can observe what's going on based on captured evidences, intentions are more subtle than behaviors. Human drivers can pass the interactions by predicting the intention of the other agents : accelerate to pass or decelerate to yield. Since humans don't perceive the world numerically, researchers have suggested that instead of calculating the distance and the speed directly to learn the time to hit an object, human drivers adopt a more cognitive and abstract methods [30].

In this work the driver behavior models is chosen for its better long-term prediction and computational efficiency compared to the other two models. Hence, in the following chapters, an explicit driver behavior models will be developed to account for driver behaviors at various traffic scenarios.

### 3 Methodology

We model the behaviors of human drivers in a simplified crossroad setup as in Fig.2 with two vehicles. The ego vehicle is moving toward the East while the surrounding vehicle is moving toward the North. Both vehicles try to cross the intersection with no signal. Let us consider only the longitudinal states with locations and velocity along the line of action without lateral movements. The lines of movement interact at the point with the symbol  $\oplus$ , we define the point as *the node* in this work.

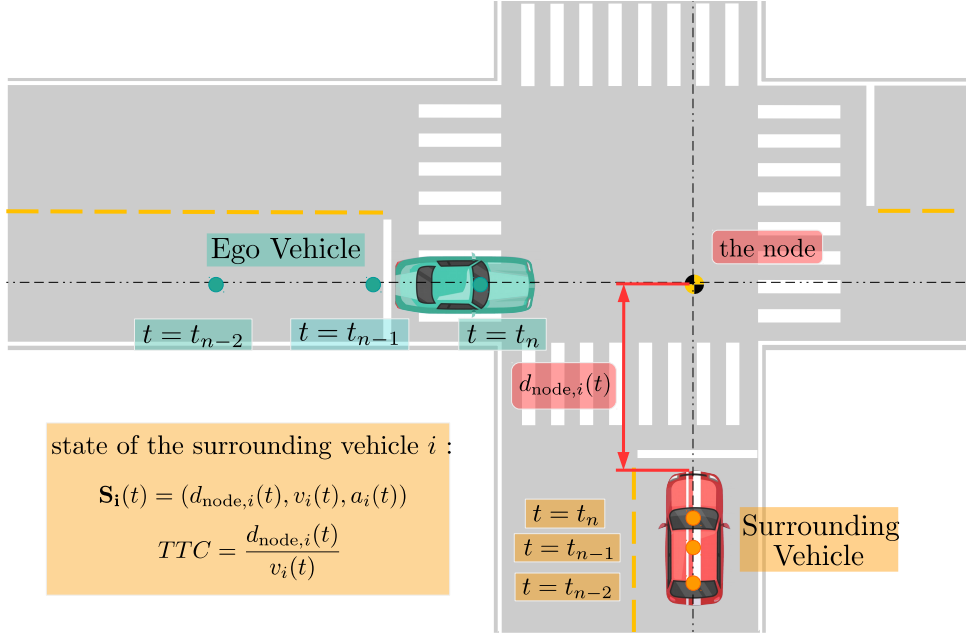


Figure 2: A scenario of two vehicles passing a crossroad with no signals

Let the node be the origin of the coordinate system with the velocity of the ego vehicle along the positive  $x$  direction, the velocity of the other agent along the positive  $y$ . The distance from the position of the  $i$ th vehicle at time  $t$  to the node is  $d_{\text{node},i}(t)$ .  $v_i(t)$  and  $a_i(t)$  are the speed and the acceleration of the vehicle  $i$  at time  $t$ , respectively. The states of each  $i$ th vehicle are defined as in Eqn.(1).

$$\mathbf{S}_i(t) = \begin{pmatrix} d_{\text{node},i}(t) \\ v_i(t) \\ a_i(t) \end{pmatrix} \quad (1)$$

The decision process on passing or yielding of the ego vehicle is shown in Fig.3. At each time instance, the states of the ego vehicle and the states of another agent are obtained. All these information are used to determine if a potential threat is present. The ego vehicle proceed with no threats, and take appropriate actions when threats are predicted. The concepts of time to collision and time for action are both introduced as the mechanisms drivers employed to determine avoid potential collisions. Apparently the time for action vary between drivers and between occasions, we therefore use probability distributions to estimate the probability of braking in Section 3.3, followed by a probabilistic evaluating model in Section 3.4. Experiments at both simulated and real environment are described in Section 3.5.

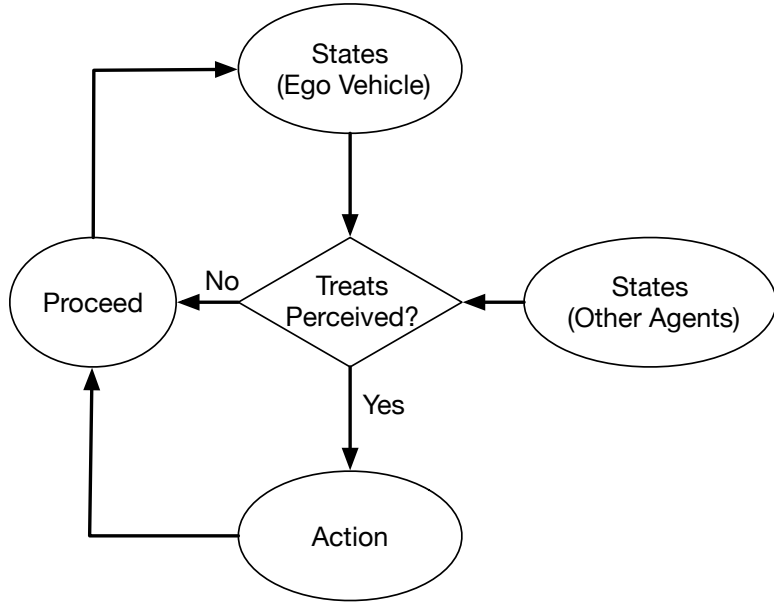


Figure 3: Pass-or-yield decision map for the ego vehicle.

### 3.1 Time to Collision

Time to Collision (TTC), or time to contact, quantifies the predicted time to collide with an obstacle ahead[31]. In traffic safety assessments, TTC is described as the time required for two vehicles to collide if they continue at their present speed, and on the same path by Hayward[32]. Experiments by Cavallo et al. in [33] also showed that TTC as described in Eqn.(2) properly drivers at different ages, genders, and experience levels when obstacles are encountered.

$$TTC = \frac{\text{distance to the node}}{\text{speed}} = \frac{d_{\text{node},i}}{v_i} \quad (2)$$

Note that  $d_{\text{node},i}$  in Eq.(2) is positive before passing the node and negative after passing the node.

### 3.2 Time for Action

The mechanism of pass-or-yield decision process of both drivers in Fig.2 unconsciously used by human drivers is defined using the parameter “Time for Action (TFA)”. TFA plays a critical role in the braking decision process by serving as a braking probability indicator of drivers. Fig. 4 illustrates an example similar to the time-history of braking in [34]. On the top of Figure 4 we have an ego vehicle approaching from the left and trying to avoid the collision at the node on the other end. At the point  $P_A$ , the car is cruising with the velocity  $v_i$ . The driver might have observed the obstacle at  $P_A$ , but determined not to take actions. Moving forward to  $P_B$  when the driver realized imminent danger and then applied the brake. The vehicle slows down and finally comes to a stop with the speed equals to 0 at point  $P_C$ . The velocity profile and the pressure on the brake in Fig.4 record the actions about the driver.

Let us look at the bottom of Fig.4 as TTC decreases as the distance to the obstacle is getting shorter. The braking decision is made at point  $P_B$  resulting a full stop at  $P_C$ . Let

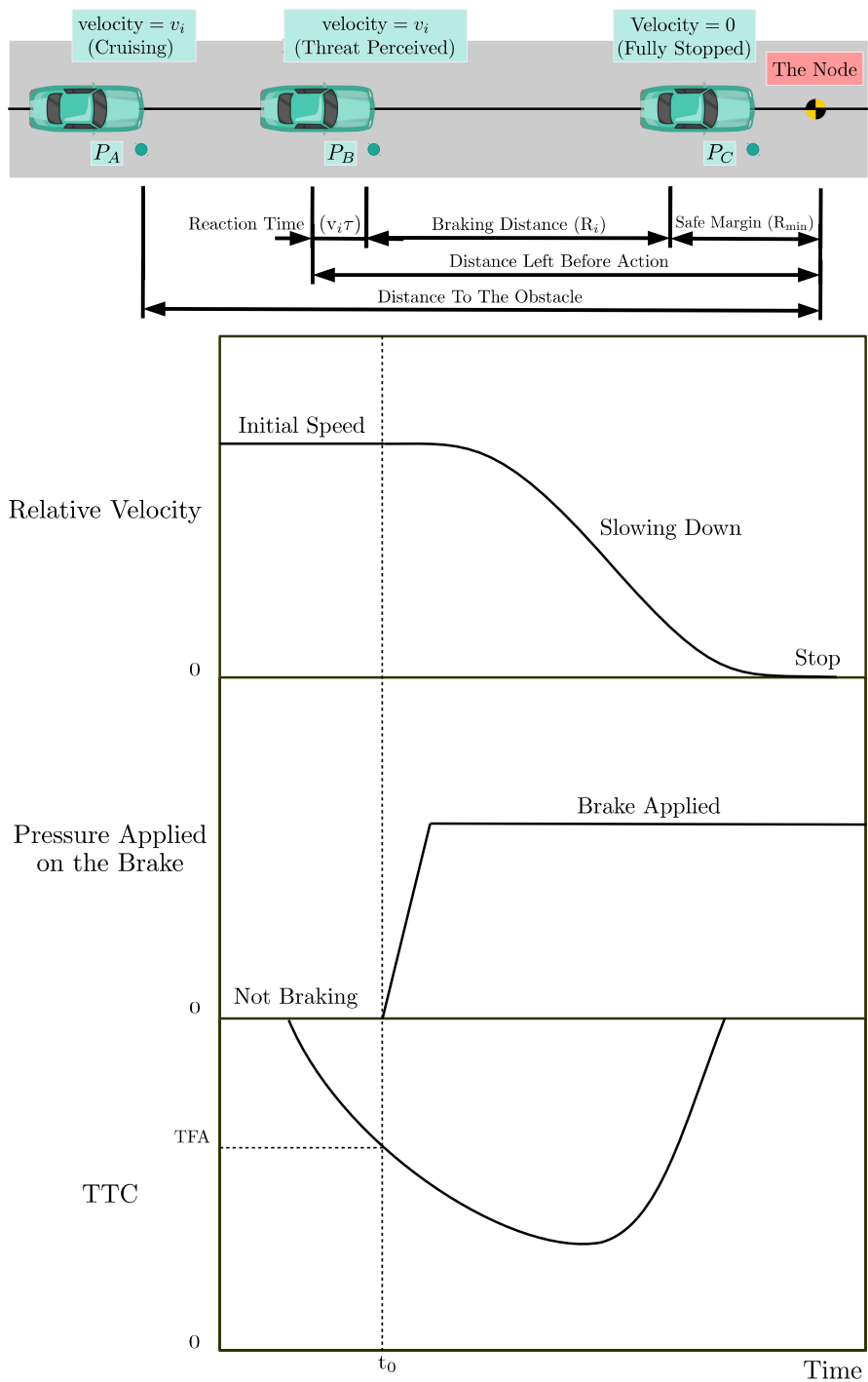


Figure 4: History of time to collision when brake is applied.

us consider the distance from  $P_B$  to the obstacle the minimum distance required to avoid collision, the time driver has to take action to avoid collision is the minimum distance divided by vehicle velocity  $v_i$ , this is defined as "Time for Action (TFA)".

TTC provide drivers a reference of when the potential collision with the obstacle might happen. The driver will hit the brake to avoid potential collision at the moment that TTC equals to TFA. This process could also be applied to the crossroad scenario when two vehicles are about to arrive at the node simultaneously. In this situation, it is foreseeable for both drivers to avoid the collision that will happen at the node, just like knowing the collision which will happen at the end of the road with the obstacle in Fig. 4. Since the node is the only a point on the intersection of these two perpendicular paths , situations for both drivers are similar to that described in Fig. 4.

### 3.3 The TFA Distribution

The TFA represents a specific TTC drivers decide to take actions, as depicted in the bottom of Fig.4. Under the most ideal situation, a driver avoids collisions by braking exactly at his/her TFA, which is the two-dots-dashed line in Fig.5. However, due to variations of human perceptions and operations, drivers only act according to current circumstances and brake somewhere close to but not exactly equal to the TFA of the driver. Hence, if we collect all the observed TFAs of a driver when he or she brakes to avoid obstacles, the two-dots-dashed lines in Fig.5 would turned into the area with slash lines in Fig.5) as the TFA uncertainty during braking.

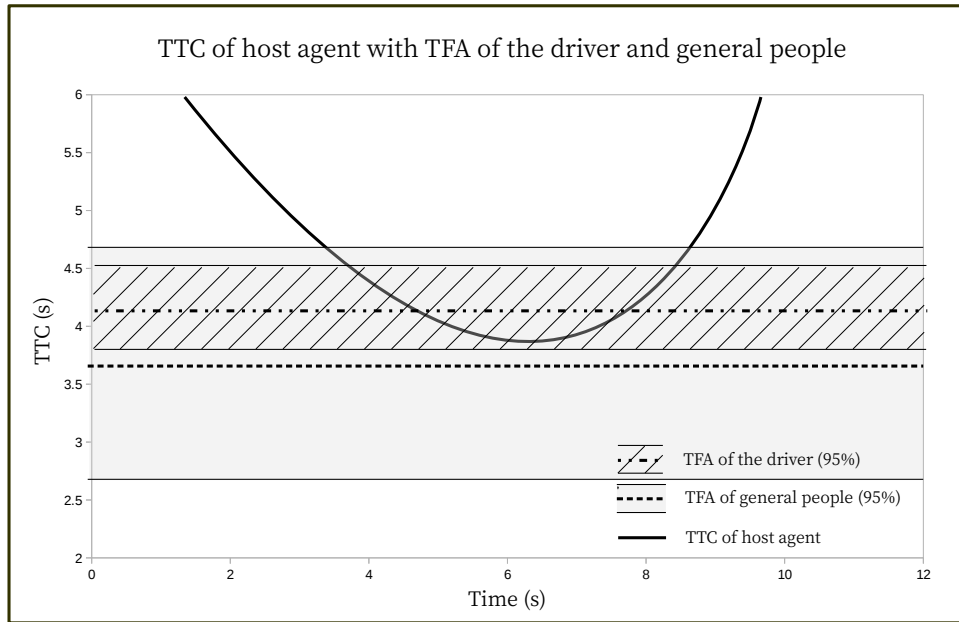


Figure 5: Example of TFA of the driver, TFA of general people and TTC of the ego vehicle.

The TFA of all drivers shall extend the TFA distribution of a single driver to a wider range to reflect inter-driver differences such as risk-taking levels as well as responses in all scenarios. For example, an aggressive driver with a high performance sports car might

have a relatively low TFA because of his personality and the short braking distance of the performance car; on the contrary, a rookie driver in an old passenger sedan might have a higher TFA with longer stopping distance. Other factors such as the state of mind when driving and reaction time could also affect TFA of a driver. The TFA distribution suggests that “within this range of TTC, some drivers will initiate the action (of braking) if potential collisions exist”. The gray band area in Fig. 5 illustrates the case when 95% of people’s TFAs are within 1.5 to 4.5 seconds with the mean value indicated by the dashed line, considering both the TFA uncertainty during braking and the TFA differences among drivers. The TTC of the ego vehicle adopted from Fig.4 is shown with a curved line. We can see that when two vehicles approach a crossroad interactions, the TTC of both drivers are reducing while the chances of braking to yield is getting higher.

We use probabilistic decision-making in modeling the interactions of two vehicles passing a crossroad. The TFA distribution with 95% interval in Fig. 5 can be re-illustrated into a probability density function (PDF), as shown in Fig. 7. At a certain value of TTC the probability of braking can promptly be obtained via integrating the PDF. For example, for a case when the TTC of a vehicle towards a crossroad is 3, the probability for the driver to brake would then be the area to the right under the PDF, which is 50%. Drivers with TFA greater than 3 would have braked before the TTC reached 3, because the displacement to the node is decreasing and the TTC drops as the ego vehicle is driven toward the crossroad according to Eqn.(2), which suggests rising of the collision risk. Hence, as the TTC gets lower, the chance for the driver to brake will increase.

The first intention to brake lies on the lowest value on the TTC curve of the ego vehicle. Let us focus on the bottom of Fig. 4 as in Fig. 6. We select three samples at  $t = 3$  seconds (squared),  $t = 5.5$  seconds (triangle), and  $t = 7$  seconds (circle). The corresponding values on the TFA distribution are shown in Fig. 7. At  $t = 3$  seconds the TTC of the ego vehicle is around 4.2 seconds. We can then estimate the probability of the vehicle stopping from the PDF in Fig. 7 as 0.13%. This result is reasonable since the TTC at this moment is still far from the TFA average. Similarly, when the  $t = 5.5$  seconds with TTC being 3.1, the probability of the vehicle stops increases to 40.1%. At  $t = 7$  seconds, since the brake is already applied, the increases in TTC will not alter the value of probability of braking. In the scenario of Fig. 6 and Fig. 7 the probability of the ego vehicle braking calculated using the lowest value on the TTC is 40.1%.

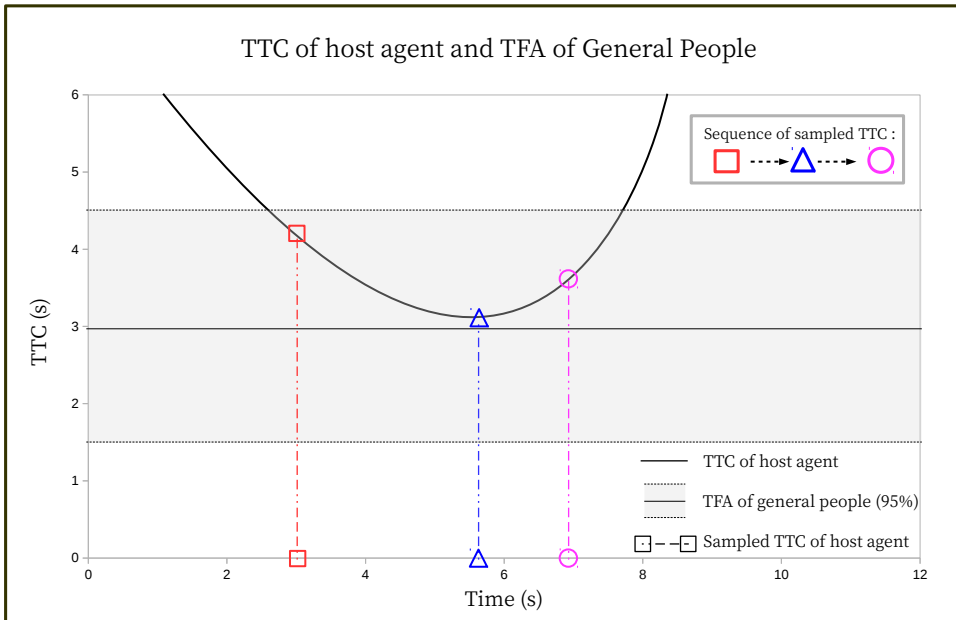


Figure 6: Example of TFA of general people and TTC of the ego vehicle.

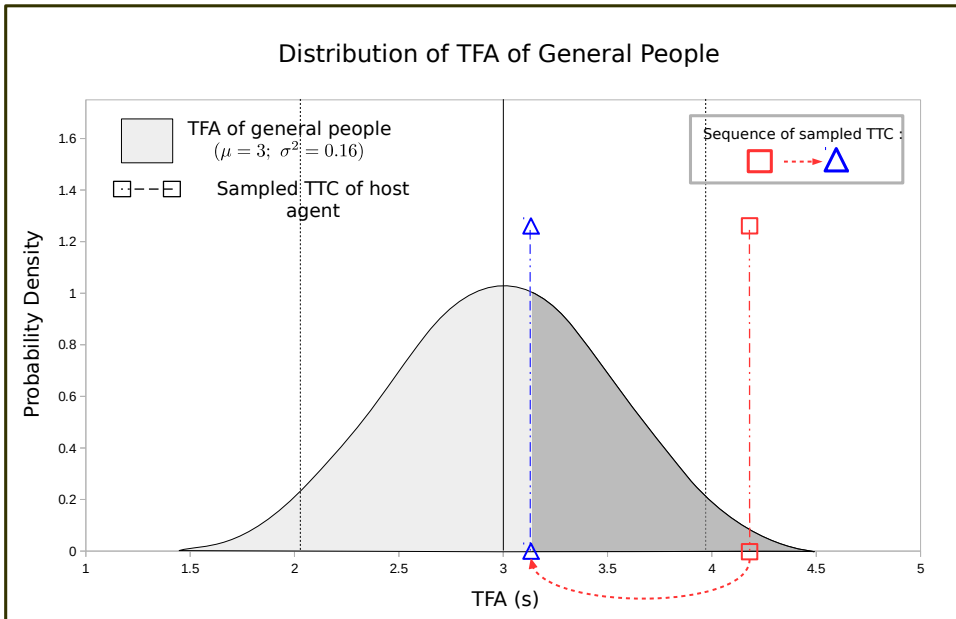


Figure 7: Example of TFA distribution of general people.

### 3.4 Mathematical Models of the Probability of Yielding

In what follows, we break down the process of braking into several parts when a driver perceives a potential danger, and formulate each part to find the TFA distribution for all drivers. Fig. 4 shows a vehicle at location  $P_A$  cruising at a velocity  $v_i$  toward the node on the right. The driver applied the brake when vehicle moves to  $P_B$ , and the vehicle fully stopped at  $P_C$  with a safe margin  $R_{\min,i}$  to the node. The overall braking distance is  $R_i$ . The vehicle travels an additional distance  $v_i\tau$  where  $\tau$  is the reaction time from the driver decided to brake to the brake engaged. The distance to the node  $d_{\text{node},i,t}$  is a function of time as vehicle moves. When a driver decides to yield,  $d_{\text{node},i,t}$  will be the distance required to fully stopped without collision, defined as the *distance left before action* in Fig. 4 .

$$\text{Distance Left Before Braking} = R_i + v_i\tau + R_{\min,i} \quad (3)$$

$$R_i = \frac{v_i^2}{2a_{\text{dec},i}} \quad (4)$$

#### 3.4.1 The distance left before action

The distance left before action is the sum of the reaction distance, the braking distance and the safe margin as shown in Eqn.(3). The reaction distance  $v_i\tau$  consider both the perception-reaction of a driver and the system actuation delay, and the reaction time  $\tau$  in this work is considered as a constant biological trait under various vehicle speeds. The braking distance is shown in Eqn.(4), where  $a_{\text{dec},i}$  is the deceleration during the brake by assuming constant deceleration throughout the entire braking process. The last parameter, safe margin, is denoted as  $R_{\min,i}$ , which stands for the safe distance that the driver left after the vehicle is fully stopped. For the sake of making data extraction easier, the  $R_{\min,i}$  is defined as distance from the center of one vehicle to another. Using the definition of TFA and Eqn.(2), we divided the distance left before braking (as in Eqn.(3)) by the speed of the vehicle  $v_i$ , TFA can then be estimated using Eqn.(5).

$$\text{TFA}_{\text{est},i} = \frac{R_i + v_i\tau + R_{\min,i}}{v_i} \quad (5)$$

In Eqn.(6) and Eqn.(7),  $R_{\min,i}$  and  $a_{\text{dec},i}$  are treated as functions of speed and are linearly formulated as Eqn, which reflect situations with different severity levels. For example, drivers might have more aggressive actions when being at lower speed (e.g. smaller  $R_{\min,i}$  for closer distance to the other vehicle after stopped) , since they believe everything is under control (i.e. the severity of the collision is low). While at high speed, drivers tend to act more conservatively (e.g. larger  $R_{\min,i}$  to keep a larger "safer margin") to avoid serious collisions.

$$R_{\min,i} = C1_{\text{Rmin},i}v_i + C2_{\text{Rmin},i} \quad (6)$$

$$a_{\text{dec},i} = C1_{\text{adec},i}v_i + C2_{\text{adec},i} \quad (7)$$

where Safe Margin Coefficient ( $C1_{\text{Rmin},i}$ ), Safe Margin Constant ( $C2_{\text{Rmin},i}$ ), Deceleration Coefficient ( $C1_{\text{adec},i}$ ), and Deceleration Constant ( $C2_{\text{adec},i}$ ) standing for the coefficients and constants of the linear equation of  $R_{\min,i}$  and  $a_{\text{dec},i}$ .

The proposed Probability of Yielding (POY) at time  $t$ , denoted as  $P_{\text{yield},i,t}$ , is shown in Eqn.(8).

$$P_{\text{yield},i,t} = \left(1 - \Phi_{\mu,\sigma^2,i}(\text{minTTC}_{i,t})\right) \quad (8)$$

where  $\text{minTTC}_{i,t}$  is the minimum TTC during the process as we discussed in Fig. 6 and Fig. 7, and  $\Phi_{\mu,\sigma^2,i}$  is the CDF of the TFA distribution, indicated by dark grey area in Fig. 7. Once we have the TFA distribution and the minimum TTC of the surrounding vehicle, we are able to calculate its POY using Eqn.(8). However, before that, some adjustment terms are required to allow the POY estimation covers all possible situations.

### 3.4.2 Adjustments for acceleration

Drivers might determine to accelerate to avoid a potential collision instead of braking. If vehicle accelerations are not taken into account, some intentions might be misunderstood. For example, a vehicle moving toward intersection with constant speed or even little acceleration would be interpreted as having the intention to brake if only the minimum TTC is considered. Let us now look at Fig. 8, from the top to the bottom are the velocity, the distance to the node, and the TTC of surrounding vehicle respectively. Fig. 8 shows a constant acceleration scenario, as the vehicle speed up, the displacement to the node drops in a parabolic curve since the vehicle is moving closer. The resulting TTC curve, defined by Eqn.(2), is also decreasing and even goes beneath 0. In the cases like this one, the POY using merely the integral from the TFA distribution, as in Fig. 7, would causing the increase of the POY as the TTC keeps decreasing.

We consider an acceleration related term  $A_{i,t}$  (Eq.(10)) as the adjusted mean value of the TFA distribution in Eq.(9).  $\alpha_{i,t}$  defines how strongly the acceleration term affects the mean value of the TFA distribution, and the  $\beta_{i,t}$  is used to prevent some disturbance introduced by sensor error or other noise. To avoid the consequences for neglecting the accelerations, the adjustments term is defined by following equations.

$$\mu_{i,t} = \text{TFA}_{\text{est},i,t} + A_{i,t} \quad (9)$$

$$A_{i,t} = \begin{cases} \alpha_{i,t} & \text{if } |\alpha_{i,t} - \alpha_{t-1,i}| < 1.67 \cdot \sigma_{\text{est}} \\ \frac{\alpha_{i,t}}{|\alpha_{i,t}|} \cdot 1.67 \cdot \sigma_{\text{est}} & \text{otherwise} \end{cases} \quad (10)$$

$$\alpha_{i,t} = \begin{cases} \beta_{i,t} \cdot \ln((|\text{TTC}'_{i,t}| + 1) \cdot e) & \text{if } \text{TTC}'_{i,t} > -1 \\ -\beta_{i,t} \cdot \ln((|\text{TTC}'_{i,t}| + 1) \cdot e) & \text{if } \text{TTC}'_{i,t} < -1 \\ \alpha_{t-1,i} & \text{otherwise} \end{cases} \quad (11)$$

$$\beta_{i,t} = \max(|\text{minTTC}_{i,t} - \text{TFA}_{\text{est},i,t}|, \sigma_{\text{est}}) \quad (12)$$

The  $\text{TTC}'_i$  (the first order derivative of TTC) in Eqn.(9) is used to take acceleration, displacement and speed into account for the POY adjustment. It is obtained from the derivative of Eqn.(2) under the assumption of constant acceleration.

$$\text{TTC}'_i = \frac{d}{dt} \frac{d_{\text{node},i}}{v_i} = -1 - a \cdot d_{\text{node},i} \cdot v_i^{-2} \quad (13)$$

We can see in Eqn.(13) that the  $\text{TTC}'_i$  equals -1 when the acceleration is 0, greater than -1 when the subject vehicle is decelerating, and less than -1 when accelerating. If

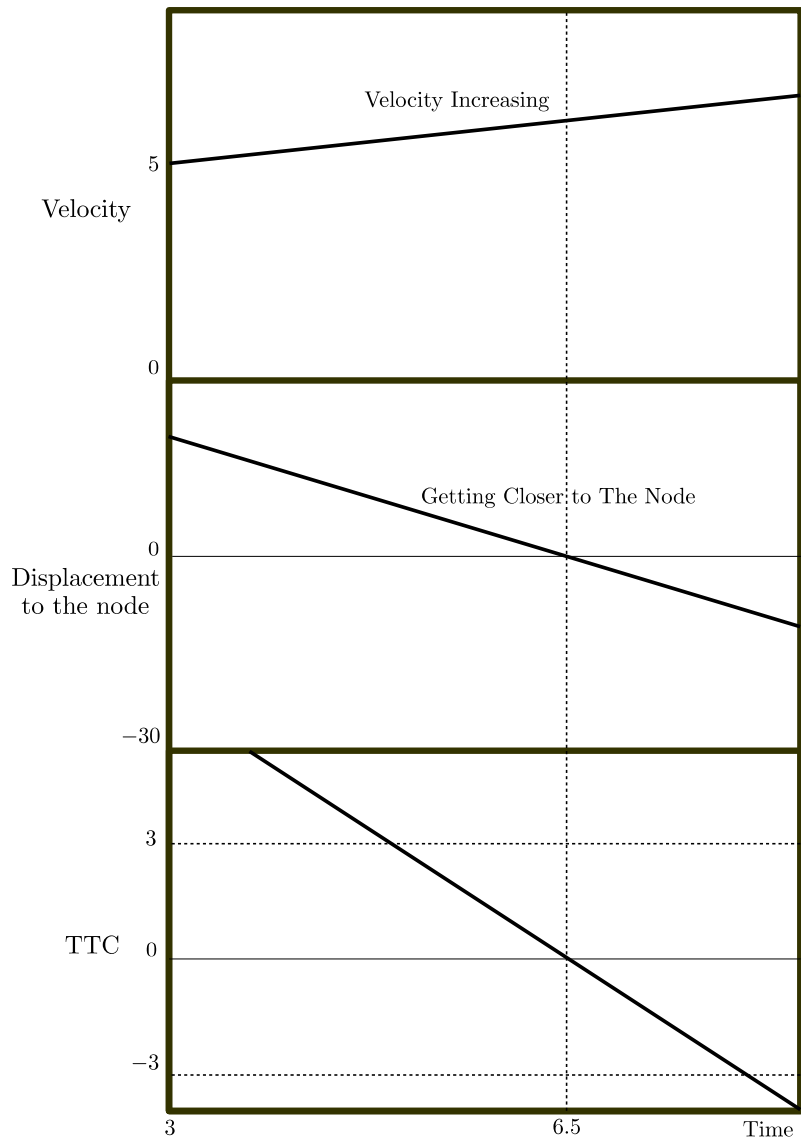


Figure 8: History of TTC as the surrounding vehicle accelerating through the node.

we bring these into Eqn.(10), we find that the mean value of the TFA distribution is increased when  $A_{i,t}$  is positive (the surrounding vehicle is decelerating), which means the resulting POY will increase under the same TTC, due to the larger integral of that area under TFA distribution, as illustrated in Fig. 9. In this figure, the current TTC equals the mean of the TFA distribution so the resulting POY is 0.5, indicated by the lighter grey area. However, since the vehicle is decelerating, the mean value of the TFA distribution is adjusted according to Eqn.(11). The POY, which is the area under the TFA distribution and right to the current TTC, becomes 0.97, shown as the darker grey area in Fig. 9.

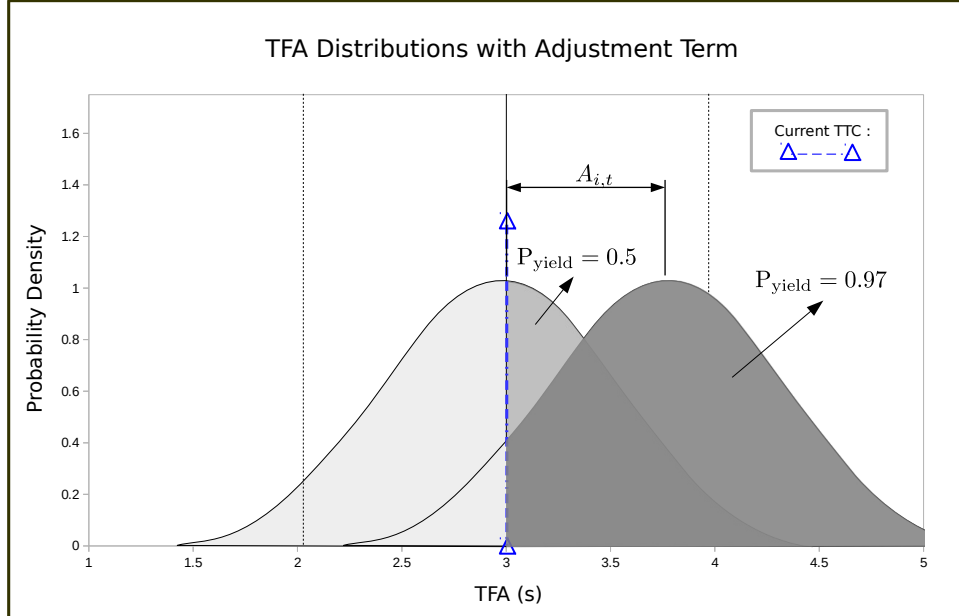


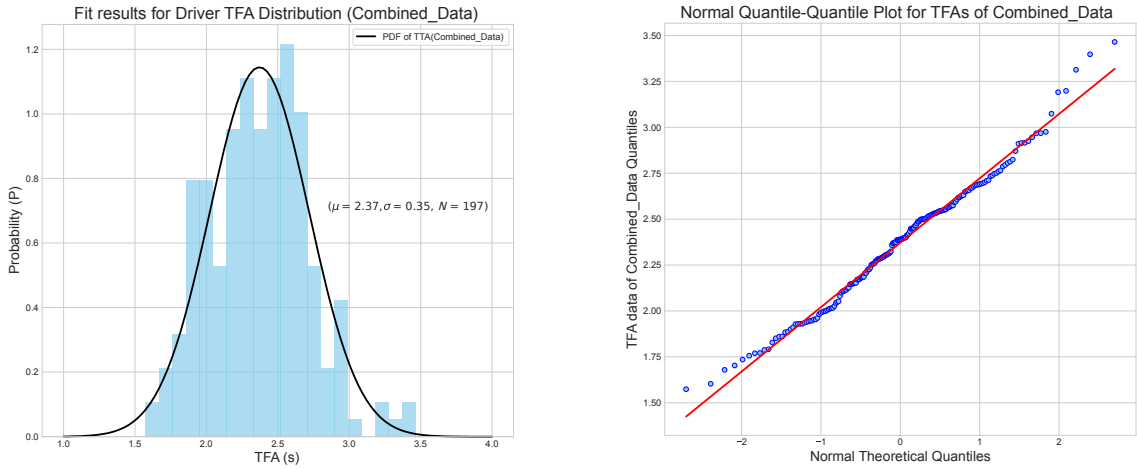
Figure 9: The effect of the weighting parameter  $A_{i,t}$  on TFA distribution.

In Eqn.(11), the magnitude of  $\alpha_t$  is adjusted depending on the greater one between  $|\min\text{TTC}_t - \text{TFA}_{\text{est},t}|$  and  $\sigma_{\text{est},t}$  (as shown in Eqn.(12)), which allows the proposed model to have more immediate response to the situation at the moment. Jagged POY curve might be shown, however, if the response is "too immediate", the maximum value of  $A_{i,t}$  is set to 1.67 standard deviation to suppress the value and prevent the POY from rising or dropping too rapidly.

### 3.4.3 TFA Distribution Parameters Estimation via Experiments

Parameters for TFA distributions are determined via a series of simulated crossroad experiments in this study. In our experiments, participants are asked to drive toward a static vehicle with constant speed and apply the brake when they believe that the collision will happen. The probability plot in Fig. 10 shows that the probability plot of the results matches a Gaussian distribution. Therefore for the remaining of the article, we assume that all TFA are Gaussian distributed, with  $\text{TFA}_{\text{est}}$  as the estimated mean value and  $\sigma_{\text{est}}$  as the standard deviation with the value 0.35.

From the experiments, we also show that  $R_{\min}$  and  $a_{\text{dec}}$  are functions of  $v_i$  and can be approximated by linear equation, which are formulated in Eqn.(6) and Eqn.(7). Fig. 11



(a) TFA distribution for all participants are displayed in histogram. The solid curve is the results approximated by Normal distribution ( $\mu = 2.37, \sigma = 0.35, N = 197$ ).

(b) Quantile-Quantile plot for the TFA distribution of the combined data against normal distribution.

Figure 10: TFA distribution of combined data fitted normally, with Quantile-Quantile plot showing its relationship with normal distribution.

and 12 shows the results of  $R_{\min}$  and  $a_{\text{dec}}$  under various velocity in our experiments. We can see that the  $R_{\min}$  does get higher linearly as the velocity rises, which is the same as predicted. Same trends happen to  $a_{\text{dec}}$  as the velocity ascends, which suggests that drivers brake slowly at low velocity and rapidly at high velocity. This result is also reasonable, since the situation tends to be more urgent when the velocity is high. Now we have all the elements needed, the required TFA distribution under different speed can now be estimated using  $TFA_{\text{est}}$ . Parameters used in the proposed TFA distribution estimation are listed in Table 2.

Table 2: Table for parameters used in TFA distribution model.

Parameters	Values
Safe Margin Coefficient ( $C1_{R_{\min}}$ )	0.295
Safe Margin Constant ( $C2_{R_{\min}}$ )	5.471
Deceleration Coefficient ( $C1_{a_{\text{dec}}}$ )	0.458
Deceleration Constant ( $C2_{a_{\text{dec}}}$ )	0.877
Reaction Time ( $\tau$ )	0.6 s

We model driver decisions at the crossroad as the probability of yielding/passing. The proposed method enables autonomous vehicles to understand the intentions of other traffic participants in a mixed-fleet environment.

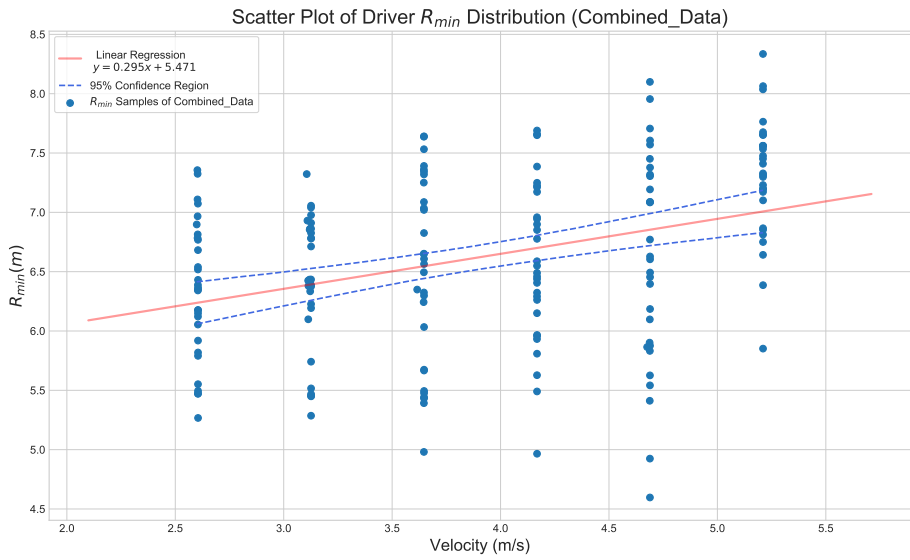


Figure 11: The  $R_{min}$  scatter plot of combined data under various velocities.

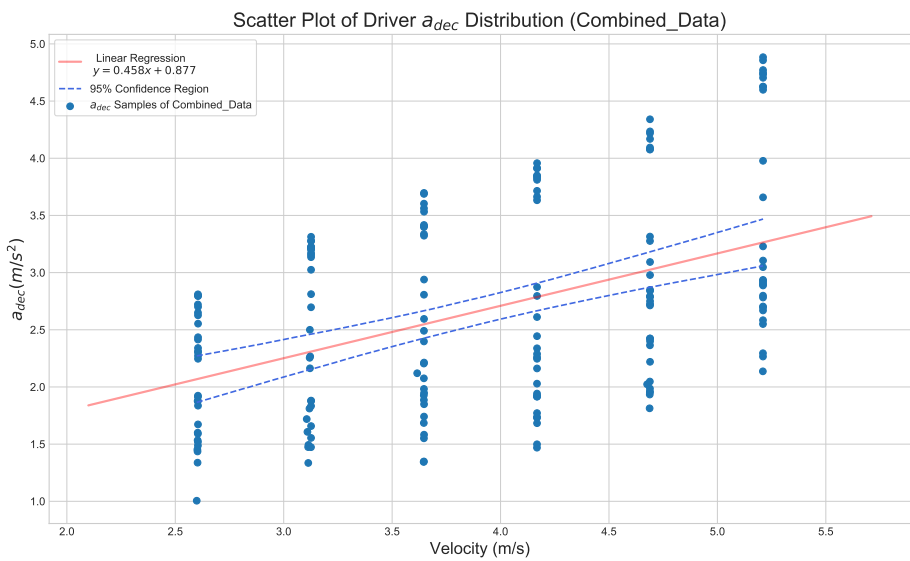


Figure 12: The  $a_{dec}$  scatter plot of combined data under various velocities.

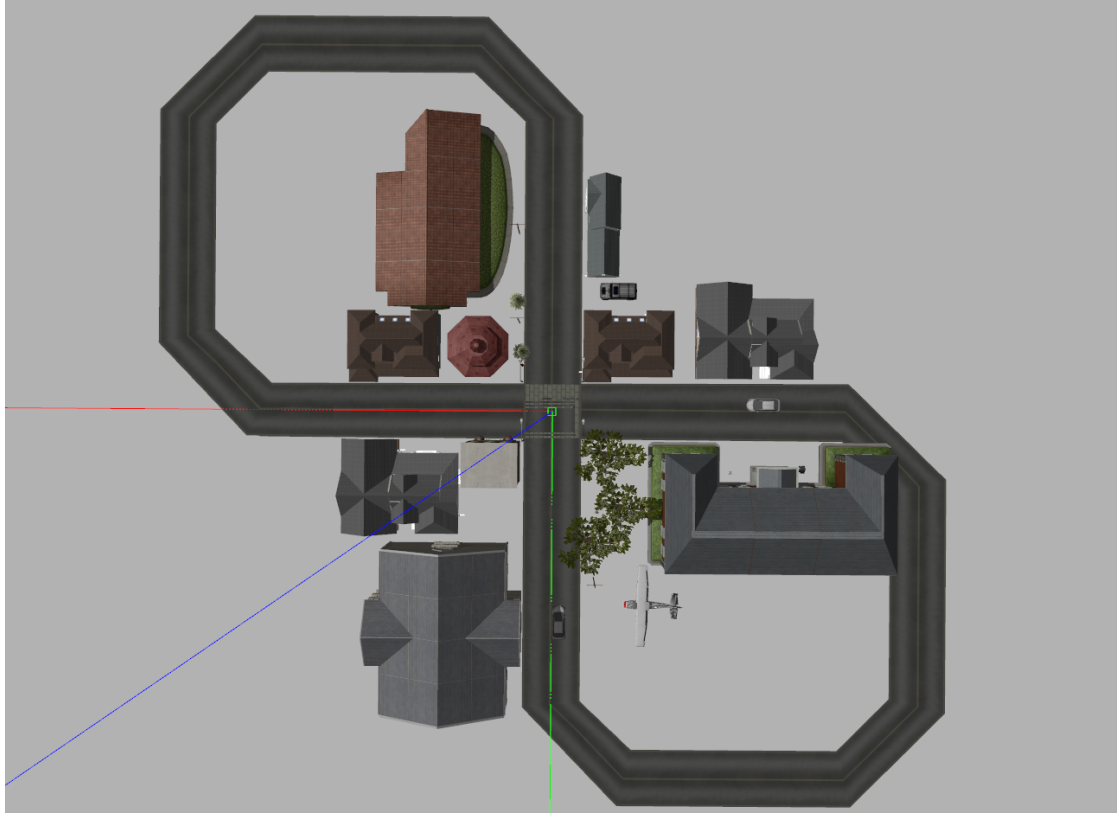


Figure 13: The simulated crossroad scenario in the Gazebo simulator.

### 3.5 Driver Intentions Prediction with Probability of Yielding

The validity of the proposed model is done at a simulated environment in Gazebo<sup>2</sup> as shown in Fig. 13. Vehicles in the virtual world are controlled through the ROS<sup>3</sup> interface. The front, left and right views from the driver seat are directly projected onto the screens when driving in simulated world as in Fig. 14c, Fig. 14a and Fig. 14b respectively. Control commands from the volunteers are sent from the joysticks to ROS node to control the simulated vehicle in Gazebo. In every set of interaction experiments, a pair of volunteers (as shown in Fig. 15a and Fig. 15b) are asked to drive across the intersection without collision. The displacements to the node and the speed of vehicles for both driver are recorded with the time resolution of 0.01 sec.

We recorded 150 sets of data (labeled with number, e.g. #001, #002, ...) with the velocity  $v_i(t)$ , and the displacement to the node  $d_{node,i}(t)$  of both vehicles. For all experiments,  $t$  begins when either of the participants is 20 meters away from the node, which is the longest distance drivers can see each other, and ends when one of the vehicle reaches the node. The corresponding TTC of car\_0 and car\_1 are then calculated, as illustrated in Fig. 16a at  $t_A, t_B, t_C, t_D$  and  $t_E$ . The probability of stopping for each car is plotted with the velocity and the displacement, as illustrated in Fig. 16b.

---

<sup>2</sup>an open source software that features 3 dimensions robotics simulator.

<sup>3</sup>short for "Robot Operating System", is a robotics middle-ware that provide users with integrated packages, services and tools



(a) Left camera from driver seat in the simulated environment.

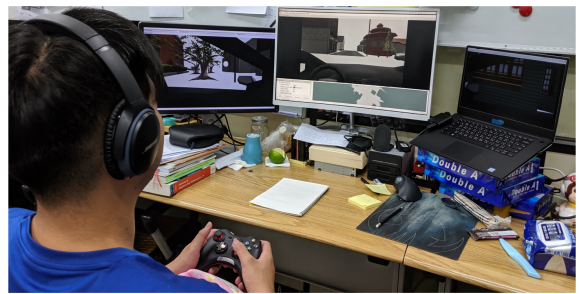


(b) Right camera from driver seat in the simulated environment.



(c) Front camera from driver seat in the simulated environment.

Figure 14: Views from driver seat in the simulated environment.

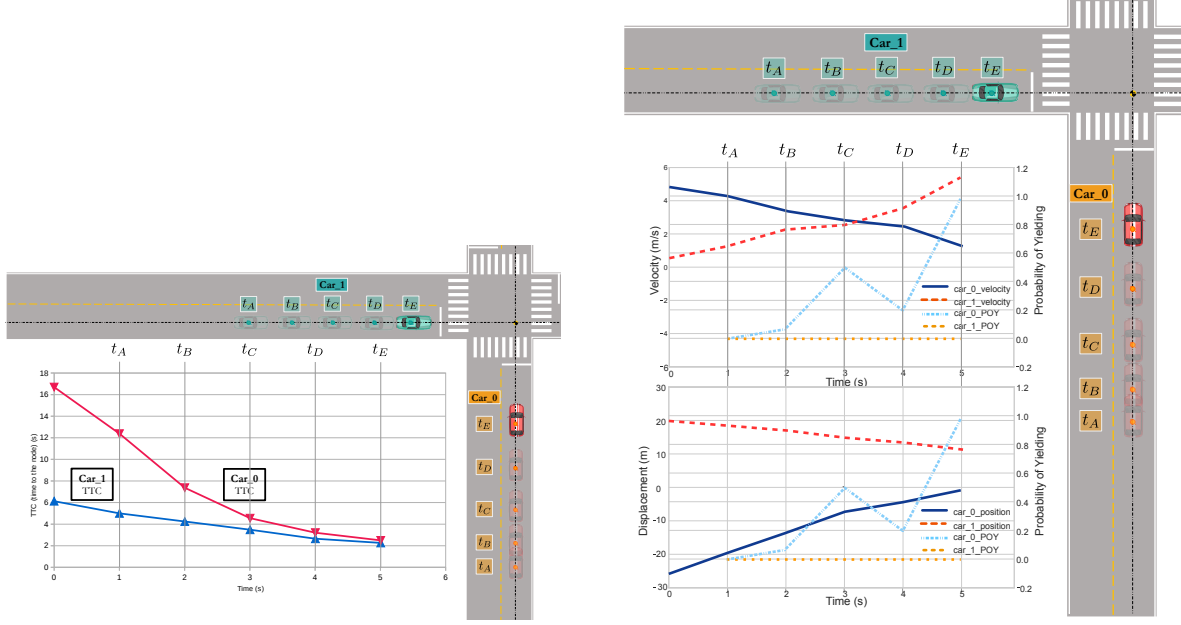


(a) First driver in the simulated crossroad interaction experiment.



(b) Second driver in the simulated crossroad interaction experiment.

Figure 15: Volunteers in the simulated crossroad interaction experiment.



(a) Illustration of calculated TTC of each vehicle.

(b) Illustration of probability of stopping together with velocity and displacement.

Figure 16: Illustration of TTC and probability of stopping along with concerning variables.

Let us look at the experiment #063 in Fig. 17. car\_0 was 21 meters to the node compared with 25 meter for car\_1. At  $t = 1.3$  seconds, the POY of car\_0 increases therefore the driver slows down to yield to car\_1 who at the moment had no intention to yield. The entire process can be reviewed clearly using POY. In this experiment without providing the POY of car\_0 to car\_1, car\_1 chose to yield too to avoid potential collision. If the intention for car\_0 is given as a reference, unnecessary braking of car\_1 could have been avoided.

Now let us look at another case #077, as shown in Fig. 18, where both drivers were indecisive without being dominate in position or other states. At the beginning of the interaction, POYs of both vehicles rose due to their deceleration. From  $t = 1.5$  to 3.2 secs, the POYs were kept at high level for car\_0, while car\_1 had no intention to yield. But right after car\_1 accelerated, so did car\_0 with very small time difference (0.5 sec). And after about a second, they both decelerated together again, but this time car\_1 was determined to yield and car\_0 finally passed. During this time, human drivers had no information about what actions the other one intended to take, so they waited until one of them did something. Yet, if one could utilize the proposed model which could estimate the TFA distribution of the driver and generate a probability from his or her current states, this stand-off-like situation could have been avoided. In the most extreme case, it will take both drivers quite a long time before either one decides to pass or yield. In trial #077, however, it did not take them too long before car\_0 finally decide to pass.

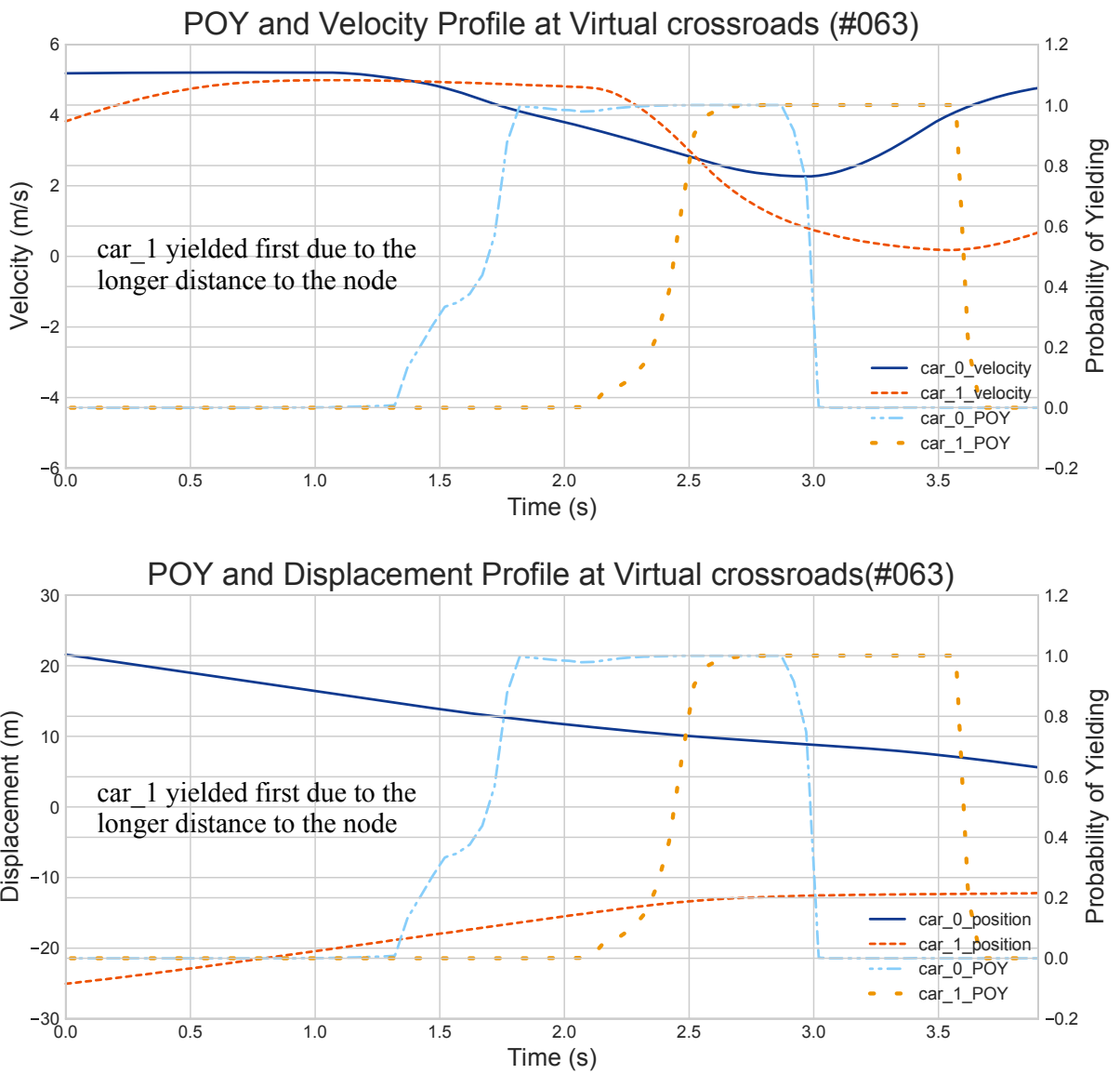


Figure 17: Trial #063 where car\_0 yielded first but then passed due to the deceleration of car\_1 .

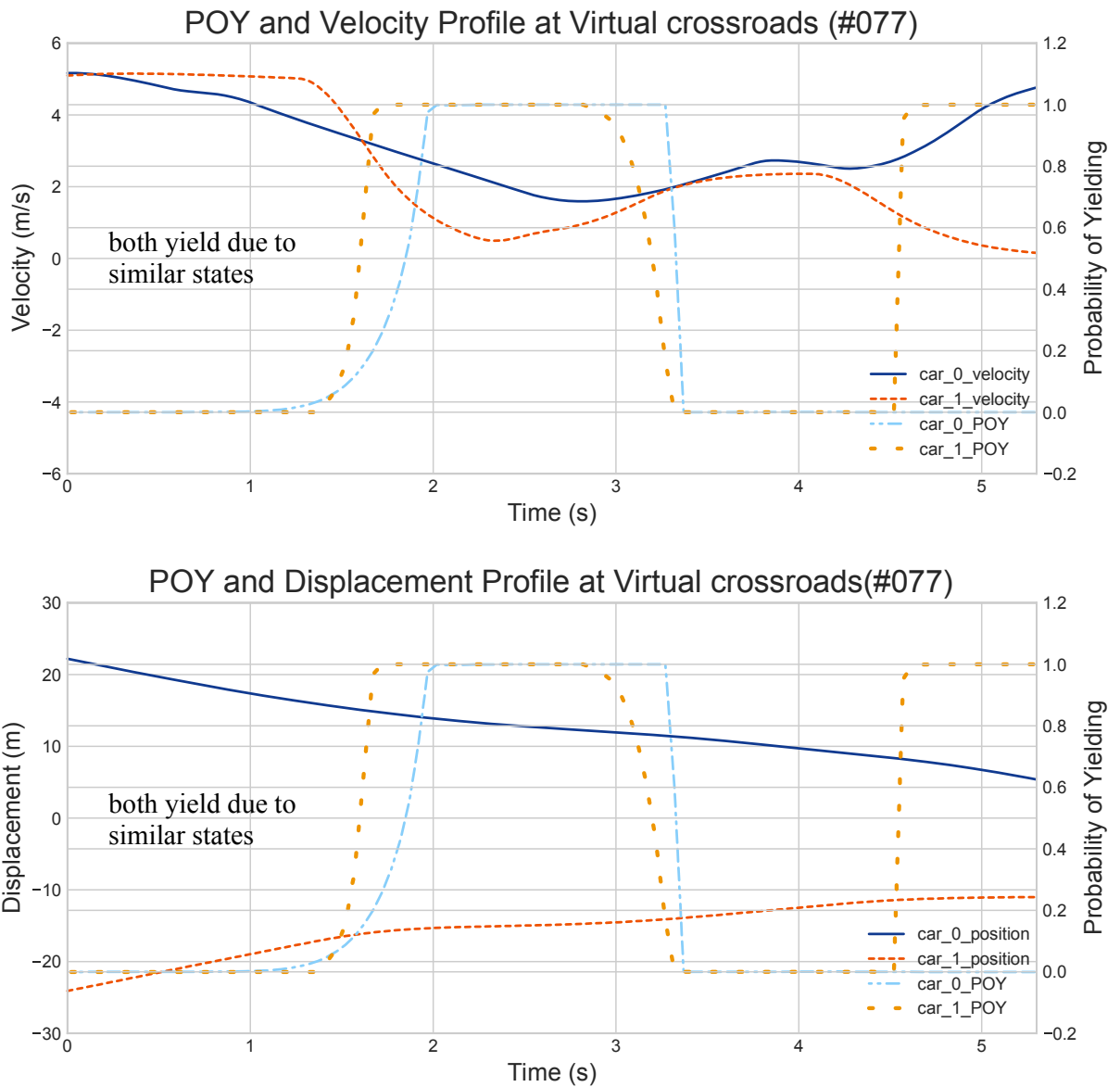


Figure 18: Trial #077 where car\_0 and car\_1 were confused about what action the other one might take.

In addition to the simulated environment, data at a real crossroad are also conducted to verify whether the proposed POY model can describe the driver behaviors in the real world. To collect the related data, the drone for aerial filming is used at the crossroad in urban environment (*Boai Rd.93-85, Yuanlin City, Changhua County 510, Taiwan* (23.958606, 120.573283)).



Figure 19: Using video analysis tool to track vehicles driven by humans.

Two of the interaction are shown in Fig. 20 and Fig. 21 where the POY curves are similar to those example trials in the virtual crossroads and are also comparable to human drivers' judgements. After examining the performance of the proposed model by comparing the POY curves to the predictions of human drivers, the accuracy of the proposed model will be examined.

$$R_{CA} = \frac{\text{number of correctly classified situations}}{\text{number of all situations}} \quad (14)$$

The  $R_{CA}$  is used to evaluate the classification accuracy of the proposed model. Due to the fact that the time spans for all interaction trials are different, the time line is reversed and denoted as  $T_{\text{minus}}$ , i.e.,  $T_{\text{minus}} = 0$  denotes the time at the end of the process and  $T_{\text{minus}} = 1$  denotes the time 1 sec earlier than that, and so on. Note that the end of the process is defined as the moment which the node is reached by one of the participants. The calculation of  $R_{CA}$  is rather straight forward as shown in Eqn.(14). In the total of 168 cases of driver behaviors at the crossroad, the denominator of the  $R_{CA}$  at each  $T_{\text{minus}}$  is then 168. The  $R_{CA}$  results of the proposed model are shown in Fig. 22.

Results using the average parameters listed in Table. 2 are plotted in solid blue line while the trend line is plotted in dashed blue line. The reason for the drop from 0.0 to 1.5  $T_{\text{minus}}$  is that, people tend to behave more aggressive in our simulated environments. During the experiment, participants who yielded for the other driver accelerated before the end of the process which is the moment when the node is reached. The example is shown in Fig. 23.

Comparing to other few behavior prediction model, the  $R_{CA}$  of the proposed model is comparable to the state-of-the-art. In the work of Graf et al. [29], the  $R_{CA}$  reached 0.81

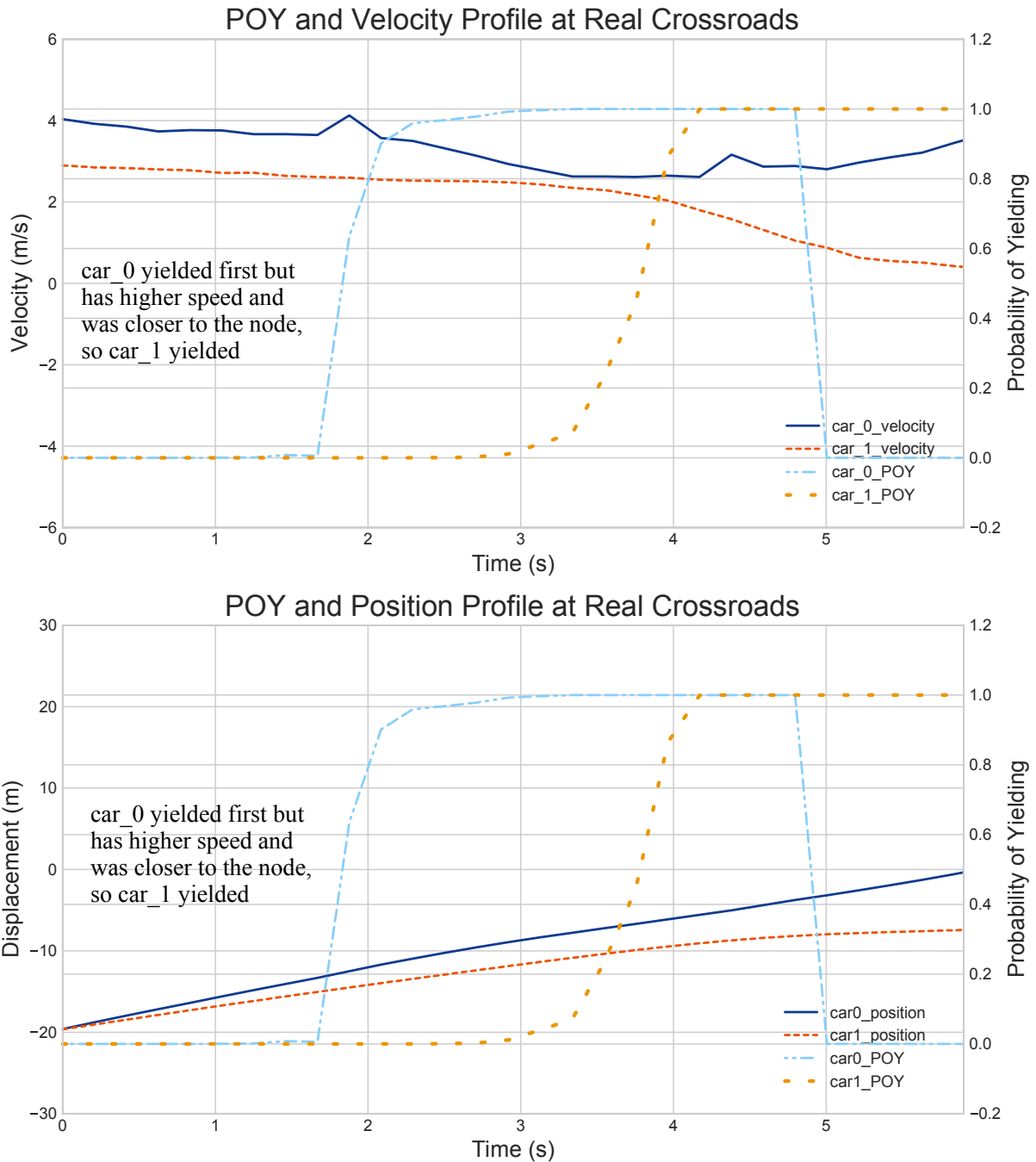


Figure 20: The corresponding POY curve at a crossroad in real world (Case I). car\_0 had the dominance position and passed at the end.

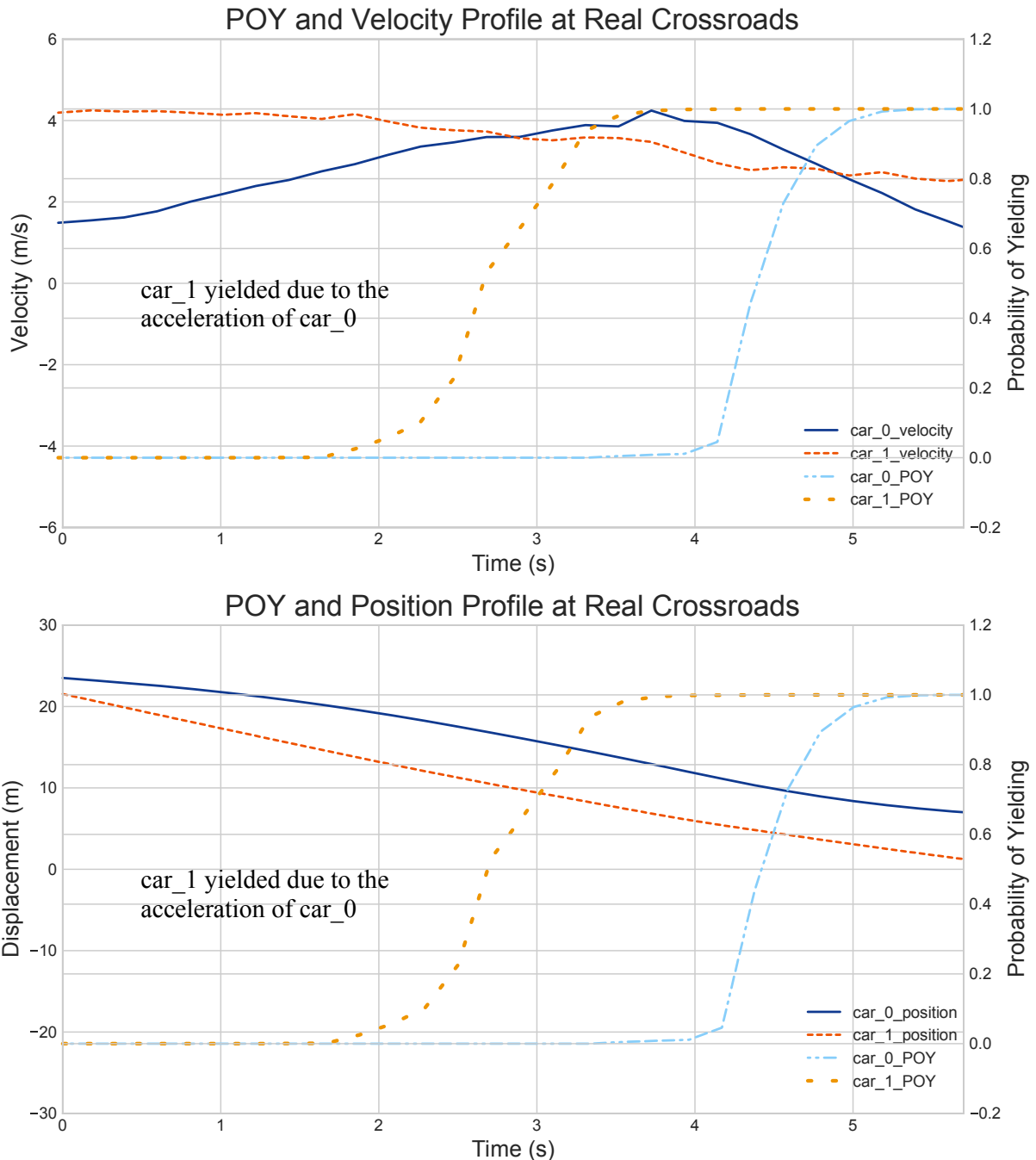


Figure 21: The corresponding POY curve at a crossroad in real world (Case II). car\_1 had the dominance position but yield at the end.

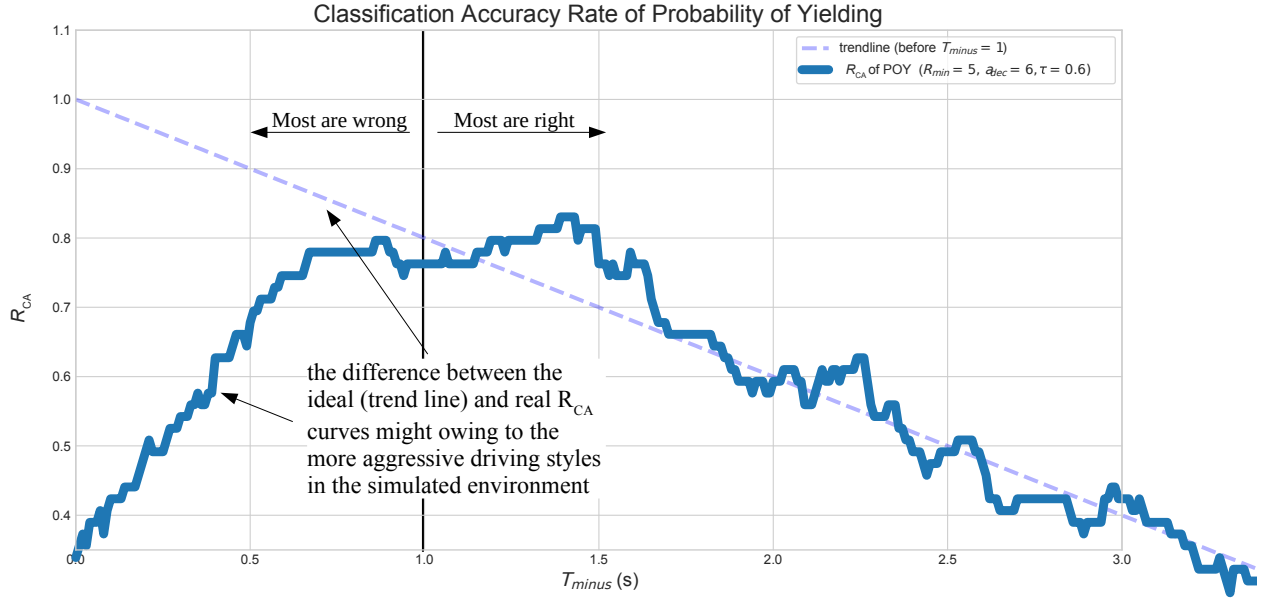


Figure 22:  $R_{CA}$  of the POY using all data sets.

at around  $T_{minus} = 3$ , while in the proposed model 0.81 is reached at  $T_{minus} = 1.5$ . This is owing to the relatively short interaction time span in the simulated environment, where participants tend to send out maximum command velocity. In the literature, interactions at real crossroads takes about 6 secs to cross a 12 to 18 meters long distance, yet at the simulated crossroad, it only takes about 3.5 secs to cross 20 meters. Furthermore, the method proposed in the literature requires pre-trained model for a specific where in POY no training steps are needed. The proposed POY also has the potential of generating better predictions if the parameters characterizing his or her driving pattern is known.

In this section, a novel driver behaviors model at crossroads was proposed. Driver intentions were predicted based on the parameter TTC, which is an important and well developed risk estimation method in traffic safety assessment. Derived form the concept, the TFA distribution was shown to be an innovative and effective driver intentions indicator that can be used to predict the driver behaviors. The normally distributed TFA distribution was then formulated and proven to be an unerring approximation. At last the driver behaviors model was finally proposed and validated at the simulated crossroad where prediction accuracy was comparable to the state-of-the-art driver behaviors prediction method.

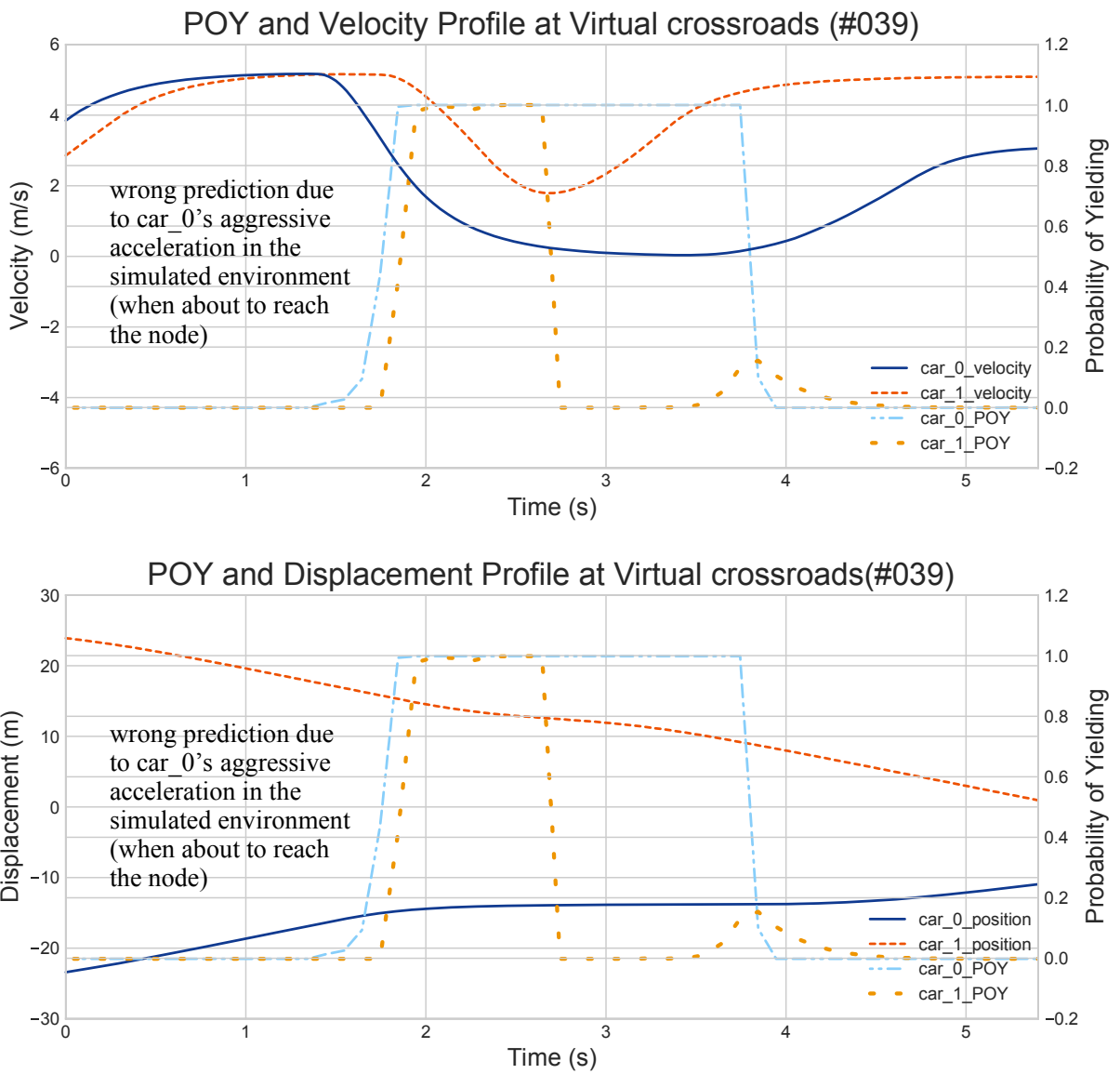


Figure 23: Example of aggressive driving pattern in simulated environment. where car\_1 begun to accelerate before car\_0 passed the node, causing the false prediction.

## 4 Extended Applications

In this section two applications using the proposed driver behavior model are explored. The first application investigates the relations between driver behaviors and traffic accidents. The proposed method show the potential to identify the rationales behind a crash and provide a probability that similar crashes will repeat. The second application identifies driver's individual parameters to better predict the behaviors using the proposed method.

### 4.1 On Crash Investigations

Although reasons behind each traffic accident vary with a broad possibilities from weather conditions to infrastructure design, traffic accidents happen more frequently in some regions and intersections. In Section 3, the TFA distribution is defined as the probability density function of the driver taking actions (e.g. braking) under different TTC. The closer the current TTC to the mean TFA of the driver, the more likely the driver will brake at this TTC. As a consequence, in the **normal** cases (where vehicles passed or yield without collisions), drivers brake at TTCs within the TFA distribution to avoid potential collisions, and most of the TTCs that drivers brake at are those being closer to the mean value of the TFA distribution (those with higher likelihood). A greater TTC value implies more conservative driving patterns and a smaller TTC value indicates more aggressive driving behaviors.

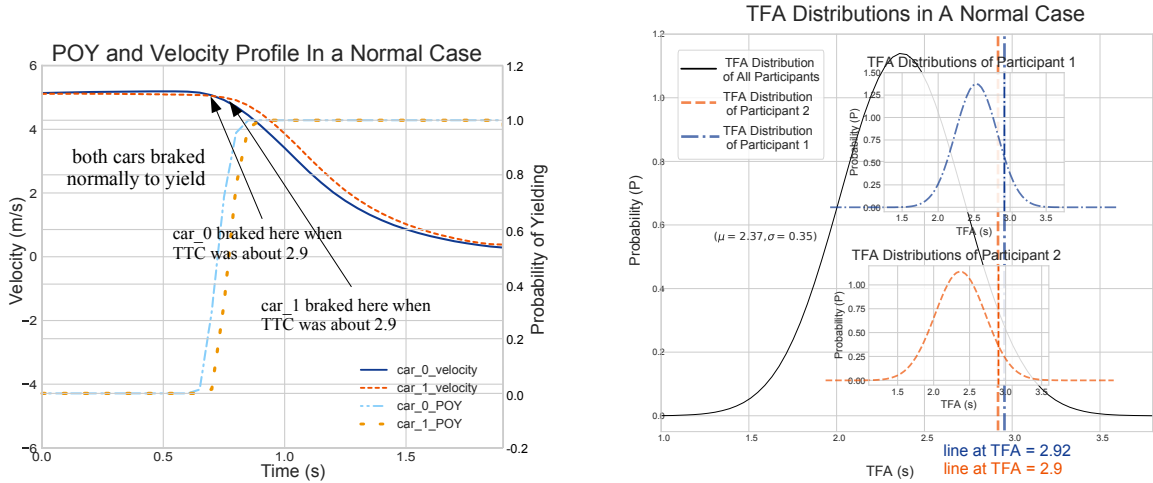
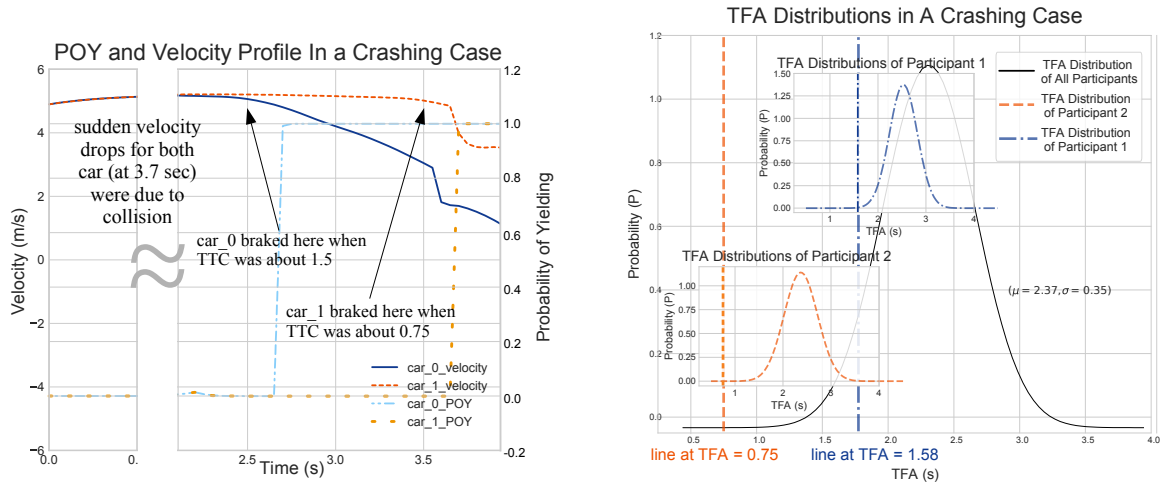


Figure 24: Velocity profile, POY and TFA distributions of participants of a case in real world where no collision happened.

Consider the TFA distributions of a normal case with no accidents as shown in Fig. 24a and Fig. 24b. The velocities and displacements of both vehicles are shown in Fig. 24a, where both vehicles yielded at around  $t = 0.7$  sec to avoid potential collisions. When looking closer at the point of braking of both vehicle, the situation at this moment could be described using the concepts of TFA distributions as shown in Fig. 24b. The TFA distribution in black solid line is the average TFA distribution of all people, as illustrated

and identified in Section 3.3. Two vertical dash lines (all-dash and dash-dot) indicate the TTCs of Car\_0 (the driver is Participant 1) and Car\_1 (the driver is Participant 2) at braking, which are 2.92 and 2.90 respectively (brakes were applied at around 0.7 sec in Fig. 24a). Sub-figures with dashed TFA distributions are the TFA distributions of Participant 1 and 2 (drivers of Car\_0 and Car\_1 respectively). In this case, both drivers brake at the TTC with relatively high likelihood (around 0.4) in the average TFA distribution.

Let us look at a case where collision happened in Fig. 25a and Fig. 25b. The velocities and displacements of both vehicles are shown in Fig. 25a, two vehicles eventually collided with each other at  $t = 3.6$  secs.



(a) The velocities versus POYs of a normal case where no collision happened. (b) TFA distributions of Participant 1, 2 and average of a normal case where a collision did happen.

Figure 25: Velocity profile, POY and TFA distributions of participants of a case in real world where collision did happen.

In Fig. 25a, driver of Car\_0 (i.e. Participant 1) believed that the other driver would yield to him, while driver of Car\_1 (i.e. Participant 2) did not even notice Car\_0 (possibly due to the lack of concentration and obstructions of his view), so they both approached to the intersection with max speed. At around 2.5 sec, Participant 1 finally braked because he realized that the collision was going to happen, and Participant 2 braked at around 3.5 sec, right before the collision. Still, the late braking did not prevent the collision from happening at around 3.6 sec. The TFA distributions of this scenario, shown in Fig. 25b, indicates that the TTCs at the moment of braking for two drivers, 0.75 for Participant 2 and 1.50 for Participant 1 respectively, have low likelihoods, both below 0.1, to brake. Both drivers' low TTCs also represent aggressive behaviors (brake at shorter distances under the same speed).

Comparing the crashing case (Fig. 25b) to the normal case where no collision happened (Fig. 24b), we can readily see that the behaviors of drivers in the crash case tend to be more aggressive (the TFAs of drivers are very low, i.e. they brake at very low TTCs) and they are also less likely to happen (very low likelihood). This finding not only shows that the concept of the proposed model is effective, but also provides a different way to examine the likelihood of accidents happening under some particular behaviors. For example, when drivers at certain crossroads are found to have braking TTCs on the far-

left side of the average TFA distribution, the possibilities of accidents in these crossroads are higher and similar scenarios are less likely to happen in a normal braking process (the TFA distribution).

## 4.2 On Driver Behavior Parameters Assessments

People have their preferred ways of driving, some are aggressive, some are conservative, and many more average drivers among us. The parameters  $R_{\min}$  and  $a_{\text{dec}}$  in TFA distributions reflect these driver behaviors: aggressive drivers tend to brake as late as possible, resulting a small  $R_{\min}$ . Similarly, drivers who drive offensively have higher  $a_{\text{dec}}$  values. Identifying an individual driver's parameters enables more accurate POY predictions, which will give rise to better classification rate  $R_{\text{CA}}$ . Let us use the term 'general parameters' to reflect the parameters for an average driver and 'individual parameters' for a specific driver we would like to study. In this section, the classification rate  $R_{\text{CA}}$  as defined in Eq.(14) will be used to determine if the individual parameters of a driver is correctly identified.

Fig. 26 shows two  $R_{\text{CA}}$  curves generated from a series of two-car crossroad interactions. Similar to Fig. 22, The  $x$ -axis is the reversed time before the end of the incident. A trend line of  $R_{\text{CA}}$  curves between  $T_{\text{minus}} = 0$  and  $T_{\text{minus}} = 1$  is plotted, showing a reasonable  $R_{\text{CA}}$  curve, where  $R_{\text{CA}}$  should be higher toward the end of the incident ( $T_{\text{minus}} = 0$ ). The solid line represents the  $R_{\text{CA}}$  curve of a driver throughout the interactions, where individual parameters are used in the POY model. The dash-dot line is the  $R_{\text{CA}}$  curve of the same driver with a different set of parameter values. We can see that using the individual parameters could effectively narrow down the TFA of the driver to within the more precise TFA distribution.

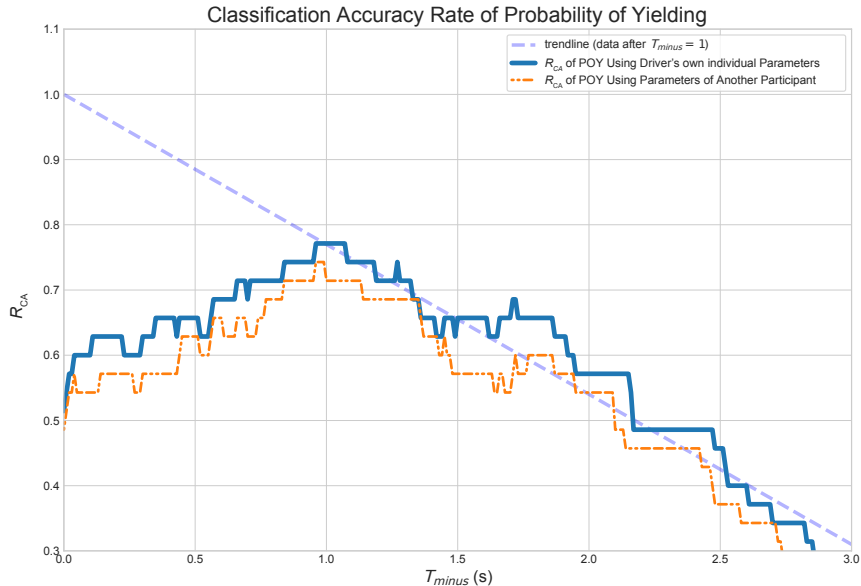


Figure 26:  $R_{\text{CA}}$  curves of POY using driver's own individual parameters and the parameters set of another participant.

Table 3: Table for individual and general parameters.

Parameters	General	Participant 1	Participant 2
Safe Margin Coefficient ( $C1_{Rmin}$ )	0.295	0.166	0.390
Safe Margin Constant ( $C2_{Rmin}$ )	5.47	6.19	5.54
Deceleration Coefficient ( $C1_{adec}$ )	0.458	0.465	0.710
Deceleration Constant ( $C2_{adec}$ )	0.877	0.377	0.813

We have shown that accurate parameters provide a better (higher)  $R_{CA}$  curve. Optimizing  $R_{CA}$  using Eq.15 could lead to the true individual parameters. The objective function in Eqn. 15 indicating our goal to maximize the total area underneath the  $R_{CA}$  curve, where the  $w$  is the parameters set. The constants  $M$  and  $N_j$  stand for the number of the trials in the collected data and the number of time steps in each trial with the resolution of 0.01 sec. The constraints in Eqn. 15 are defined by the minimum and maximum values of  $R_{min}$  and  $a_{dec}$  in the simulated environment, which are the distances between two cars and acceleration capabilities, respectively. In this study, we use Simulated Annealing (SA) due to the non-smooth and time-consuming properties of the objective function.

$$\begin{aligned}
 & \underset{w}{\text{minimize}} \quad \frac{1}{M} \sum_{j=1}^M \sum_{i=1}^{N_j} -f(\text{POY}_j(t_i, w)) \\
 & \text{subject to} \quad 2.0 \cdot C1_{Rmin} + C2_{Rmin} \geq 4.48, \\
 & \quad 5.2 \cdot C1_{Rmin} + C2_{Rmin} \leq 12.0, \\
 & \quad 2.0 \cdot C1_{adec} + C2_{adec} \geq 0.01, \\
 & \quad 5.2 \cdot C1_{adec} + C2_{adec} \leq 3.5
 \end{aligned} \tag{15}$$

where the function  $\text{POY}_j$  in the optimization problem is

$$f(\text{POY}_j) = \begin{cases} 1 & \text{if } \text{POY}_j(t, w) \geq 0.8 \text{ and yielded} \\ 1 & \text{if } \text{POY}_j(t, w) \leq 0.2 \text{ and passed} \\ 0 & \text{otherwise} \end{cases} \tag{16}$$

The values 2.0 and 5.2 are the minimum and maximum velocities right before braking. While the values 4.48 and 12.0 is calculated from the distances between centers of two vehicles, one is the closest between the two and the other the furthest (right before braking). 0.01 and 3.5 are the acceleration boundaries.

The results of the optimization are shown in Table 4 and Fig. 27, and the parameters used for the Simulated Annealing (SA) in the optimization problem are listed in Table 5. The optimized parameters do have a better  $R_{CA}$  curve, but the corresponding optimized parameters are quite different from that of the participant's true parameters. This might be owing to that the optimized parameter set is over sensitive to accelerations. Note that all five optimized results are overlapped together. To improve the optimization, modifications of the objective function could be a possible solution.

Our proposed POY model can identify possible reasons behind each crash, especially for those associated directly with driver behaviors. We are able to evaluate the intentions of drivers at crossroads and the results are similar to those observed and verified in the

Table 4: Table for results of the proposed optimization problem.

<b>Optimization Number</b>	$C1_{Rmin}$	$C2_{Rmin}$	$C1_{adec}$	$C2_{adec}$	<b>Area</b>
1st Optimization	0.362	7.91	0.0460	0.954	-205.40
2nd Optimization	0.401	7.86	0.224	0.563	-205.37
3rd Optimization	0.322	7.91	0.106	0.941	-205.23
4th Optimization	0.456	7.49	0.102	0.824	-205.37
5th Optimization	0.346	7.95	0.145	0.812	-205.37
<b>individual</b>	<b>0.166</b>	<b>6.19</b>	<b>0.465</b>	<b>0.377</b>	<b>-183.89</b>

Table 5: Table for parameters used in the Simulated Annealing.

<b>Parameters</b>	<b>Values</b>
Start Temperature	120
End Temperature	0.02
Steps	100000

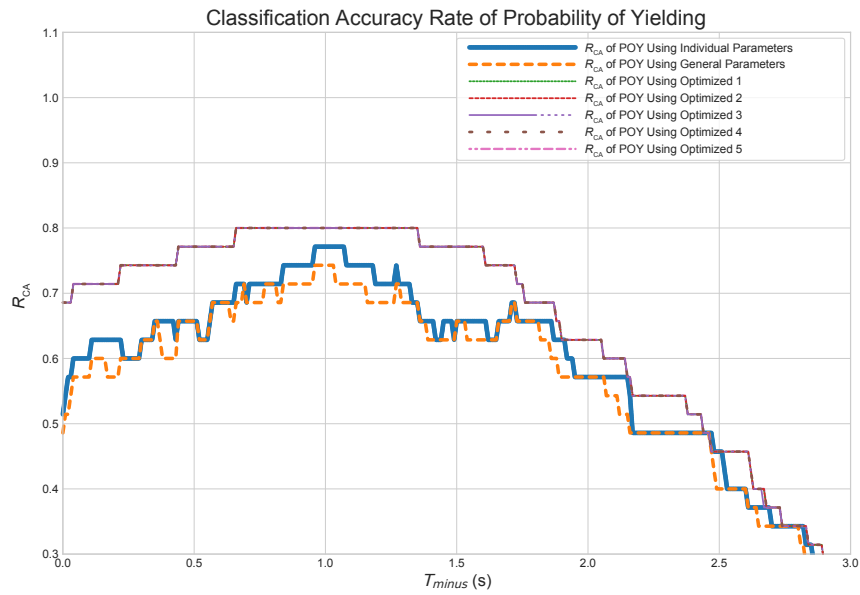


Figure 27:  $R_{CA}$  curve of POY using characteristic parameters and optimized parameters are plotted.

simulated environment. The POY model also helps determine traffic characteristic parameters using optimization techniques. Although our results only provide a preliminary study on how to identify local traffic individuals, we show potential the practicality of the POY model in diverse extended applications.

## 5 Concluding Remarks

In this research, the behaviors of human drivers were modeled in a probability measure of yield based on the cognitive information. The proposed POY enables a formal formulation of human driving decision processes. Experiments conducted in both simulated and urban environments also support the idea by showing predictions similar to that of human drivers. The classification accuracy rate using the proposed model is also comparable to the state-of-the-art method.

We extend the proposed model to traffic risk assessments and driver behavior parameters identifications. Under reasonable assumptions the preliminary attempts to assess the safety of crossroads as well as to identify different driving style are explored. These possible applications show how the proposed model could be further developed to help improving the road safety using the TFA distribution and the prediction results.

The contexts of the presented work assume 1) the TTC is the major role in human drivers' cognitive behaviors in the simplified crossroad model; 2) the TFA being normally distributed under available verification. In the future, the proposed model will be extended for multi-agent joint behaviors predictions to form a more realistic prediction model. The parameter identification would also be modified to enhance the reliability and robustness of parameter identification. The average parameters of an area can not only gives us the driving styles of the area, but also help autonomous vehicles with adjusted judgements of the possible behaviors of the neighborhood. The work presented can help building a computer driving logic that matches human behaviors such that interactions between different drivers will be more intuitive.

## References

- [1] S. Thrun, M. Montemerlo, H. Dahlkamp, D. Stavens, A. Aron, J. Diebel, P. Fong, J. Gale, M. Halpenny, G. Hoffmann, et al. Stanley: The robot that won the darpa grand challenge. *Journal of field Robotics*, 23(9):661–692, 2006.
- [2] J. Walker and C. Johnson. Peak car ownership: The market opportunity of electric automated mobility services. Technical report, 2016. Accessed: 2019-06-23.
- [3] California Department of Motor Vehicles. Report of traffic collision involving an autonomous vehicle (ol 316), 2019.
- [4] P. Bansal and K. Kockelman. Forecasting americans long-term adoption of connected and autonomous vehicle technologies. *Transportation Research Part A: Policy and Practice*, 95:49 – 63, 2017.
- [5] US Department of Transportation. Preparing for the future of transportation: Automated vehicles 3.0 (av 3.0). Technical report, sep 2018. Accessed: 2019-06-23.

- [6] K. Dresner and P. Stone. Sharing the road: Autonomous vehicles meet human drivers. pages 1263–1268, 01 2007.
- [7] S.I. Guler, M. Menendez, and L. Meier. Using connected vehicle technology to improve the efficiency of intersections. *Transportation Research Part C: Emerging Technologies*, 46:121 – 131, 2014.
- [8] D. Milakis, M. Snelder, B. Arem, B. Wee, and G. Homem de Almeida Correia. Development and transport implications of automated vehicles in the netherlands: scenarios for 2030 and 2050. *European Journal of Transport and Infrastructure Research*, 17(1), 2017.
- [9] A. Millard-Ball. The autonomous vehicle parking problem. *Transport Policy*, 75:99 – 108, 2019.
- [10] T Litman. Autonomous vehicle implementation predictions: Implications for transport planning. Technical report, Victoria Transp. Policy Inst., Victoria, BC, Canada, 2015.
- [11] E. Coelingh, A. Eidehall, and M. Bengtsson. Collision warning with full auto brake and pedestrian detection - a practical example of automatic emergency braking. In *13th International IEEE Conference on Intelligent Transportation Systems*, pages 155–160, Sep. 2010.
- [12] S. Bonnin, T. H. Weisswange, F. Kummert, and J. Schmuedderich. Pedestrian crossing prediction using multiple context-based models. In *17th International IEEE Conference on Intelligent Transportation Systems (ITSC)*, pages 378–385, Oct 2014.
- [13] F. Schneemann and P. Heinemann. Context-based detection of pedestrian crossing intention for autonomous driving in urban environments. In *2016 IEEE/RSJ International Conference on Intelligent Robots and Systems (IROS)*, pages 2243–2248, Oct 2016.
- [14] Y. Hashimoto, Y. Gu, L.T. Hsu, M. Iryo-Asano, and S. Kamijo. A probabilistic model of pedestrian crossing behavior at signalized intersections for connected vehicles. *Transportation Research Part C: Emerging Technologies*, 71:164 – 181, 2016.
- [15] S. Ramyar, M. G. Sefidmazgi, S. Amsalu, A. Anzagira, A. Homaifar, A. Karimoddini, and A. Kurt. Modeling driver behavior at intersections with takagi-sugeno fuzzy models. In *2015 IEEE 18th International Conference on Intelligent Transportation Systems*, pages 2378–2383, Sep. 2015.
- [16] V. Gadepally, A. Krishnamurthy, and U. Ozguner. A framework for estimating driver decisions near intersections. *IEEE Transactions on Intelligent Transportation Systems*, 15(2):637–646, April 2014.
- [17] B. Paden, M. áp, S. Z. Yong, D. Yershov, and E. Frazzoli. A survey of motion planning and control techniques for self-driving urban vehicles. *IEEE Transactions on Intelligent Vehicles*, 1(1):33–55, March 2016.
- [18] S. Lefèvre, D. Vasquez, and C. Laugier. A survey on motion prediction and risk assessment for intelligent vehicles. *ROBOMECH Journal*, 1(1):1–14, 2014.

- [19] S. Ammoun and F. Nashashibi. Real time trajectory prediction for collision risk estimation between vehicles. In *2009 IEEE 5th International Conference on Intelligent Computer Communication and Processing*, pages 417–422, Aug 2009.
- [20] P. Fiorini and Z. Shiller. Motion planning in dynamic environments using velocity obstacles. *The International Journal of Robotics Research*, 17(7):760–772, 1998.
- [21] W. Zhan, C. Liu, C. Chan, and M. Tomizuka. A non-conservatively defensive strategy for urban autonomous driving. In *2016 IEEE 19th International Conference on Intelligent Transportation Systems (ITSC)*, pages 459–464, Nov 2016.
- [22] M. Ruf, J. Ziehn, B. Rosenhahn, J. Beyerer, D. Willersinn, and H. Gotzig. Situation prediction and reaction control (sparc). In B. Färber, K. Dietmayer, K. Bengler, M. Maurer, Ch. Stiller, and H. Winner, editors, *9. Workshop Fahrerassistenzsysteme (FAS 2014)*, pages 55–66, Walting im Altmühlthal, Germany, March 2014.
- [23] S. Lefèvre, C. Laugier, and J. Ibañez-Guzmán. Evaluating risk at road intersections by detecting conflicting intentions. In *2012 IEEE/RSJ International Conference on Intelligent Robots and Systems*, pages 4841–4846, Oct 2012.
- [24] I. Dagli, M. Brost, and G. Breuel. Action recognition and prediction for driver assistance systems using dynamic belief networks. In JG. Carbonell, J. Siekmann, R. Kowalczyk, JP. Müller, H. Tianfield, and R. Unland, editors, *Agent Technologies, Infrastructures, Tools, and Applications for E-Services*, pages 179–194, Berlin, Heidelberg, 2003. Springer Berlin Heidelberg.
- [25] T. Gindele, S. Brechtel, and R. Dillmann. Learning context sensitive behavior models from observations for predicting traffic situations. In *16th International IEEE Conference on Intelligent Transportation Systems (ITSC 2013)*, pages 1764–1771, Oct 2013.
- [26] A. Foka and P. Trahanias. Probabilistic autonomous robot navigation in dynamic environments with human motion prediction. *International Journal of Social Robotics*, 2(1):79–94, Mar 2010.
- [27] C. Hubmann, J. Schulz, M. Becker, D. Althoff, and C. Stiller. Automated driving in uncertain environments: Planning with interaction and uncertain maneuver prediction. *IEEE Transactions on Intelligent Vehicles*, 3(1):5–17, March 2018.
- [28] M. Liebner, M. Baumann, F. Klanner, and C. Stiller. Driver intent inference at urban intersections using the intelligent driver model. In *2012 IEEE Intelligent Vehicles Symposium*, pages 1162–1167, June 2012.
- [29] R. Graf, H. Deusch, F. Seeliger, M. Fritzsche, and K. Dietmayer. A learning concept for behavior prediction at intersections. In *2014 IEEE Intelligent Vehicles Symposium Proceedings*, pages 939–945, June 2014.
- [30] A. Kemeny and F. Panerai. Evaluating perception in driving simulation experiments. *Trends in Cognitive Sciences*, 7(1):31 – 37, 2003.
- [31] J. Caird and P. Hancock. The perception of arrival time for different oncoming vehicles at an intersection. *Ecological Psychology*, 6(2):83–109, 1994.

- [32] J. Hayward. Near miss determination through use of a scale of danger. *Report TTSC-7115*, 1972.
- [33] V. Cavallo and M Laurent. Visual information and skill level in time-to-collision estimation. *Perception*, 17(5):623–632, 1988. PMID: 3249670.
- [34] W. Winsum and W. Brouwer. Time headway in car following and operational performance during unexpected braking. *Perceptual and Motor Skills*, 84(3\_suppl):1247–1257, 1997. PMID: 9229443.